



## RESEARCH ARTICLE

10.1002/2017GC007153

## Key Points:

- Elevated Hg and Hg/TOC values occur at the stratigraphic levels of the Mid-Cenomanian Event and Oceanic Anoxic Event 2
- Small Hg signals are consistent with Hg dispersal by a submarine plume, following a subaqueous LIP emplacement, rather than atmospheric dispersion

## Supporting Information:

- Supporting Information S1
- Table S1

## Correspondence to:

J. D. Scaife,  
james.scaife@linacre.ox.ac.uk

## Citation:

Scaife, J. D., Ruhl, M., Dickson, A. J., Mather, T. A., Jenkyns, H. C., Percival, L. M. E., . . . Minisini, D. (2017). Sedimentary mercury enrichments as a marker for submarine large igneous province volcanism? Evidence from the Mid-Cenomanian event and Oceanic Anoxic Event 2 (Late Cretaceous). *Geochemistry, Geophysics, Geosystems*, 18, 4253–4275. <https://doi.org/10.1002/2017GC007153>

Received 24 JUL 2017

Accepted 24 OCT 2017

Accepted article online 1 NOV 2017

Published online 1 DEC 2017

Corrected 15 JAN 2018

This article was corrected on 15 JAN 2018. See the end of the full text for details.

# Sedimentary Mercury Enrichments as a Marker for Submarine Large Igneous Province Volcanism? Evidence From the Mid-Cenomanian Event and Oceanic Anoxic Event 2 (Late Cretaceous)

J. D. Scaife<sup>1</sup> , M. Ruhl<sup>1</sup> , A. J. Dickson<sup>1,2</sup> , T. A. Mather<sup>1</sup> , H. C. Jenkyns<sup>1</sup> , L. M. E. Percival<sup>1,3</sup>, S. P. Hesselbo<sup>4</sup>, J. Cartwright<sup>1</sup>, J. S. Eldrett<sup>5</sup>, S. C. Bergman<sup>6</sup> , and D. Minisini<sup>7</sup>

<sup>1</sup>Department of Earth Sciences, University of Oxford, Oxford, UK, <sup>2</sup>Now at Department of Earth Sciences, Royal Holloway University of London, Egham, Surrey, UK, <sup>3</sup>Now at Institute of Earth Sciences, Géopolis, University of Lausanne, Lausanne, Switzerland, <sup>4</sup>Camborne School of Mines and Environment and Sustainability Institute, University of Exeter, Penryn, UK, <sup>5</sup>Shell International Exploration & Production B.V., Rijswijk, GS, the Netherlands, <sup>6</sup>Now at Shell R&D Houston, Vashon, WA, USA, <sup>7</sup>Shell International Exploration and Production Inc., Houston, TX, USA

**Abstract** Oceanic Anoxic Event 2 (OAE 2), during the Cenomanian-Turonian transition (~94 Ma), was the largest perturbation of the global carbon cycle in the mid-Cretaceous and can be recognized by a positive carbon-isotope excursion in sedimentary strata. Although OAE 2 has been linked to large-scale volcanism, several large igneous provinces (LIPs) were active at this time (e.g., Caribbean, High Arctic, Madagascan, Ontong-Java) and little clear evidence links OAE 2 to a specific LIP. The Mid-Cenomanian Event (MCE, ~96 Ma), identified by a small, 1‰ positive carbon-isotope excursion, is often referred to as a prelude to OAE 2. However, no underlying cause has yet been demonstrated and its relationship to OAE 2 is poorly constrained. Here we report sedimentary mercury (Hg) concentration data from four sites, three from the southern margin of the Western Interior Seaway and one from Demerara Rise, in the equatorial proto-North Atlantic Ocean. We find that, in both areas, increases in mercury concentrations and Hg/TOC ratios coincide with the MCE and the OAE 2. However, the increases found in these sites are of a lower magnitude than those found in records of many other Mesozoic events, possibly characteristic of a marine rather than atmospheric dispersal of mercury for both events. Combined, the new mercury data presented here are consistent with an initial magmatic pulse at the time of the MCE, with a second, greater pulse at the onset of OAE 2, possibly related to the emplacement of LIPs in the Pacific Ocean and/or the High Arctic.

## 1. Introduction

The mid-Cretaceous was a period characterized by major perturbations in the global carbon cycle, associated with the widespread development of anoxic–euxinic conditions in the global ocean, termed Oceanic Anoxic Events (OAEs) (Arthur et al., 1987; Jenkyns, 1980, 2010; Schlanger et al., 1987; Schlanger & Jenkyns, 1976). One widely studied anoxic event, Oceanic Anoxic Event 2 (OAE 2, Cenomanian-Turonian, ~94 Ma) is typically marked by the appearance of organic-rich mudstones, often referred to as “black shales.” It is recorded in many parts of the world’s oceans and marked by a globally recognized positive carbon-isotope excursion (CIE) and other anomalies (Tsikos et al., 2004). This positive CIE is thought to reflect the widespread burial of relatively <sup>12</sup>C-enriched organic matter in marine sediments, and the development of anoxic/euxinic conditions in many marine basins (Dickson et al., 2016, 2017; Jarvis et al., 1988; Jenkyns, 2010; Schlanger et al., 1987; Sinninghe Damsté & Köster, 1998). This study focuses on the southern Western Interior Seaway and Demerara Rise in the proto-southern North Atlantic (Figure 1). However, in contrast to other globally recognized sections that recorded organic-rich deposits developed under anoxic to euxinic conditions during the OAE 2 interval (e.g., Bonarelli Level in Europe), some parts of the southern Western Interior Seaway recorded relatively organic-lean sediments deposited during oxygenated conditions (e.g., Eldrett et al., 2014, 2017; Meyers, 2007). On Demerara Rise “black shales” occur throughout the Albian-Santonian stages and are not limited to the OAE 2 level (Erbacher et al., 2004; Meyers et al., 2006; Shipboard Scientific Party, 2004).

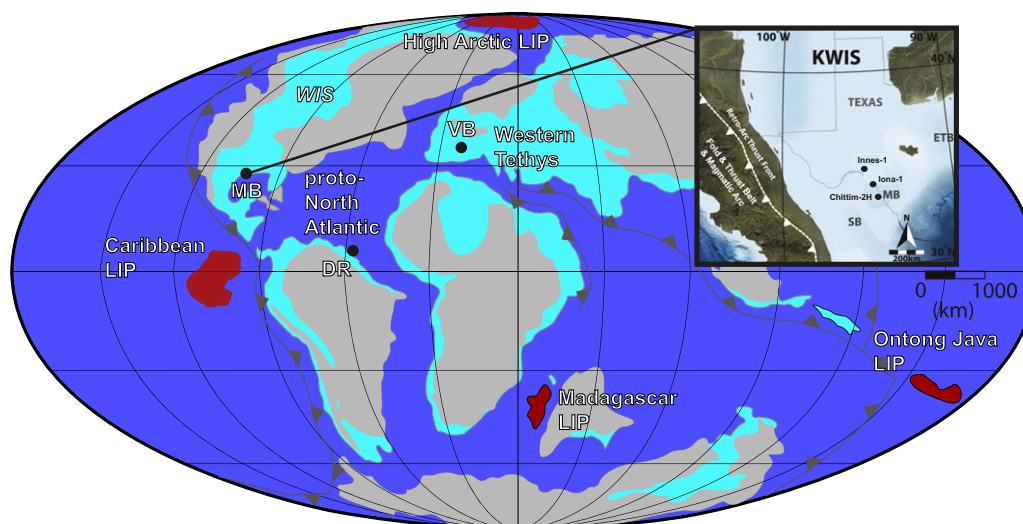


**Figure 1.** Map showing the positions of the Caribbean, High Arctic and Madagascar LIPs during the Cenomanian-Turonian time interval, as well as the Western Interior Seaway (WIS), Maverick Basin (MB), Demerara Rise (DR), and the Vocontian Basin (VB). The Caribbean LIP formed as the result of an oceanic hot spot through the Farallon Plate at near equatorial latitudes during 100–87 Ma (Luzieux et al., 2006) creating an oceanic plateau, Rio Cala intraoceanic plateau and numerous scattered intrusions (Spikings et al., 2015). The formation of the Madagascar LIP relates to the Marion hot spot (Storey et al., 1995). However, the precise timing, which has been suggested to range from 31 to 97 Ma, is poorly constrained (Mahoney et al., 1991; Storey et al., 1995; Torsvik et al., 1998). The High Arctic LIP formed following the Jurassic opening of the Canada Basin (130–80 Ma; tholeiitic volcanism) (Brown et al., 1987; Bailey & Rasmussen, 1997; Corfu et al., 2013; Davis et al., 2017; Estrada, 2015; Estrada & Henjes-Kunst, 2004; Evenchick et al., 2015; Polteau et al., 2015). Magmatic successions of the High Arctic LIP are observed in the Canadian Arctic Islands, Svalbard, Franz Josef Land, Chukchi, Barents Shelf, Alpha-Mendeleev Rise, and in North Greenland (see Buchan & Ernst, 2006; Maher, 2001). The Ontong Java LIP forms part of the largest known oceanic plateau and LIP, the Ontong Java-Manihiki-Hikurangi Plateau complex in the Pacific Ocean (Bryan and Ernst, 2008; Taylor, 2006). The Ontong Java LIP formed between 25 and 119 Ma as the result of an intra-plate oceanic hot-spot (Bryan & Ernst, 2008; Mahoney et al., 1993; Neal et al., 1997; Tejada et al., 1996, 2002, 2004). Light blue shading indicates shallow marine, dark blue indicates deep-marine, and gray indicates terrestrial environments. Dark gray lines with chevrons indicate a convergent margin. This figure includes a close-up of the Cretaceous Western Interior Seaway (KWIS; top right) displaying the position of the Maverick Basin cores (SB-Sabinas Basin; ETB-East Texas Basin; Figure modified after Du Vivier et al., 2014 and Eldrett et al., 2014).

The Cenomanian-Turonian OAE 2 is also globally marked by changes in assemblages of planktonic and benthonic calcareous microbiota, such as foraminifers and ostracods, as well as dinoflagellates, nannofossils, and, locally, radiolarians (Coccioni et al., 2016; Eldrett et al., 2017; Erba, 2004; Falzoni et al., 2016; Jarvis et al., 1988; Musavu-Moussavou et al., 2007). In northern Europe, invasion of boreal “pulse faunas,” including the belemnite species *Praeactinocamax plenus*, was a feature of the early to midphase of OAE 2, suggesting at least regional cooling; this is also reflected in increases in bulk oxygen-isotope values of enclosing chalks signifying a fall in surface-water temperatures (Gale & Christensen, 1996; Jenkyns et al., 2017; Lamolda et al., 1994). This so-called Plenus Cold Event was also registered in the western Atlantic and at the southern end of the Western Interior Seaway by invasion of boreal dinoflagellates (Eldrett et al., 2014; van Helmond et al., 2014), as well as by falls in temperature in the proto-Atlantic determined by the organic geochemical TEX<sub>86</sub> proxy (Forster et al., 2007; Sinninghe Damsté et al., 2010). The global nature of the Plenus Cold Event is signified by a drop in  $p\text{CO}_2$  reconstructed from organic geochemical proxies, stomatal indices of fossil leaves, and the relative difference between changes in carbonate and organic-carbon isotopes (Barclay et al., 2010; Jarvis et al., 2011; Kuypers et al., 1999). Overall, the pattern of extinctions and originations, also involving macrobiota such as ammonites and bivalves, is significant enough to have originally defined the Cenomanian-Turonian stage boundary (Jarvis et al., 1988).

The global carbon cycle was also perturbed during the Mid-Cenomanian Event (MCE), which is marked by a  $\sim 1\text{‰}$  positive carbon-isotope excursion in sediment carbonate fractions. The size of this excursion is slightly smaller, and shorter in duration, than the  $\sim 2\text{--}3\text{‰}$  positive CIE recorded during OAE 2 (Eldrett et al., 2015a; Gambacorta et al., 2015; Jarvis et al., 2006; Joo & Sageman, 2014). Integrated astronomical age models from

the Western Interior Seaway date the onset of the MCE to  $96.57 \pm 0.12$  Ma, the peak of the first MCE carbon-isotope excursion known as MCE 1a at  $96.49 \pm 0.15$  Ma (the second carbon-isotope excursion peak of the MCE is known as MCE 1b) and the end of the MCE to  $96.36 \pm 0.12$  Ma (Batenburg et al., 2016; Eldrett et al., 2015a). Comparatively, age models from the Western Interior Seaway for OAE 2 estimate the start of the initial carbon-isotope excursion at around  $94.65 \pm 0.12$  Ma and the duration of the whole OAE between 0.52 and 0.71 Myr. This duration can, however, be extended to 0.92 Ma following a more inclusive interpretation of the isotopic onset of the event as well as the recognition that many sections contain an unconformity at the base of the CIE (Eldrett et al., 2015a, 2017; Ma et al., 2014; Sageman et al., 2006).

Sections of mid-Cenomanian age in the Western Interior Seaway and equatorial Atlantic show a modest increase in values of total organic carbon (TOC) during the MCE, suggesting that accelerated global organic-matter burial also drove the positive carbon-isotope excursion during this event (Figure 2, cf. Friedrich et al., 2009). Like OAE 2, the MCE was also typified by changes in assemblages of benthic and planktonic foraminifers and radiolarians (Coccioni & Galeotti, 2003). Equally, carbonate sections recording the MCE show the presence, in brachiopod calcite, of relatively heavy oxygen-isotope ratios that suggest cooling, and are locally accompanied by boreal “pulse faunas” including the belemnite *Praeactinocamax primus*, the form ancestral to *Praeactinocamax plenus* (Gale & Christensen, 1996; Mitchell & Carr, 1998; Paul et al., 1994; Voigt et al., 2004). Nd-isotope evidence suggests a climatically controlled reorganization of water masses during both the MCE and OAE 2, at least in northern European and adjacent areas (Zheng et al., 2016).

Detailed geochemical studies (iodine:calcium ratios of pelagic carbonates and iron-speciation studies of interbedded organic-rich black shales) of one section in Marche-Umbria, Italy, suggest that both subsurface and bottom waters were characterized by relatively low dissolved oxygen contents in the interval between the MCE and OAE 2 (Owens et al., 2017), but there are no significant carbon-cycle events except for a minor positive CIE recorded in the English Chalk named the “Jukes-Browne Event.” This event can be correlated with a similar small-scale feature in the Western Interior Seaway (Jarvis et al., 2006; Joo & Sageman, 2014).

Extensive volcanic activity and the subaqueous emplacement of Large Igneous Provinces (LIPs) (Caribbean, High Arctic, Madagascar, and Ontong-Java LIPs: Figure 1) have previously been suggested to be responsible for the initiation of OAE 2 and the MCE. The most significant evidence for volcanism during OAE-2 is a distinct shift towards unradiogenic osmium-isotope ratios, which predates the onset of the Cenomanian-Turonian positive CIE by  $10^1$ – $10^2$  kyr and suggests that a major pulse of volcanism and associated seafloor hydrothermal weathering began prior to its onset (Figure 6; Du Vivier et al., 2014, 2015; Jenkyns et al., 2017; Orth et al., 1993; Snow et al., 2005; Tegner et al., 2011; Turgeon & Creaser, 2008). The associated, potentially large-scale, release of greenhouse gases and other compounds is suggested to have resulted in the initiation of a number of catastrophic and interconnected oceanographic and climatic changes (Blättler et al., 2011; Erbacher et al., 2001; Pogge von Strandmann et al., 2013; van Helmond et al., 2013). However, the dynamic nature and spatial heterogeneity of the responses to volcanism at the time of OAE 2 are poorly constrained. For example, decreases in redox-sensitive trace metals throughout large areas of the Western Interior Seaway indicate it may have become destratified and ventilated during OAE 2 despite water column stratification and stagnation occurring in many other parts of the global oceans (Eldrett et al., 2014, 2017). Furthermore, palynological assemblages display increases in gymnosperms through the Plenus Cold Event interval, possibly reflecting a transition from megathermal to mesothermal vegetation and potentially indicating a period of climatic cooling rather than an increased hydrological cycle (Eldrett et al., 2017; van Helmond et al., 2014).

Thus far, linking the initiation of OAE 2 to a specific magmatic event has relied on the temporal coincidence of LIP emplacement (Caribbean, High Arctic, Madagascar, and Ontong-Java LIPs: Figure 1) with proposed environmental changes. However, changing lead-isotopic ratios in marine strata that record OAE 2 at Gorgo a Cerbara (Marche-Umbria, Italy) show a shift toward values tentatively associated with the Caribbean and Madagascar LIPs, in addition to mid-ocean ridge basalts (MORB) (Kuroda et al., 2007). Alternatively, if the invasion of boreal biota during the Plenus Cold Event involved the southward movement of water masses, the Arctic LIP may have been an important source for observed geochemical changes in marine sediments (Zheng et al., 2013).

Mercury (Hg) enrichments in sedimentary successions are increasingly showing promise as a tracer for major volcanic events in the past. Events studied include the end-Permian, end-Triassic, Early Toarcian,

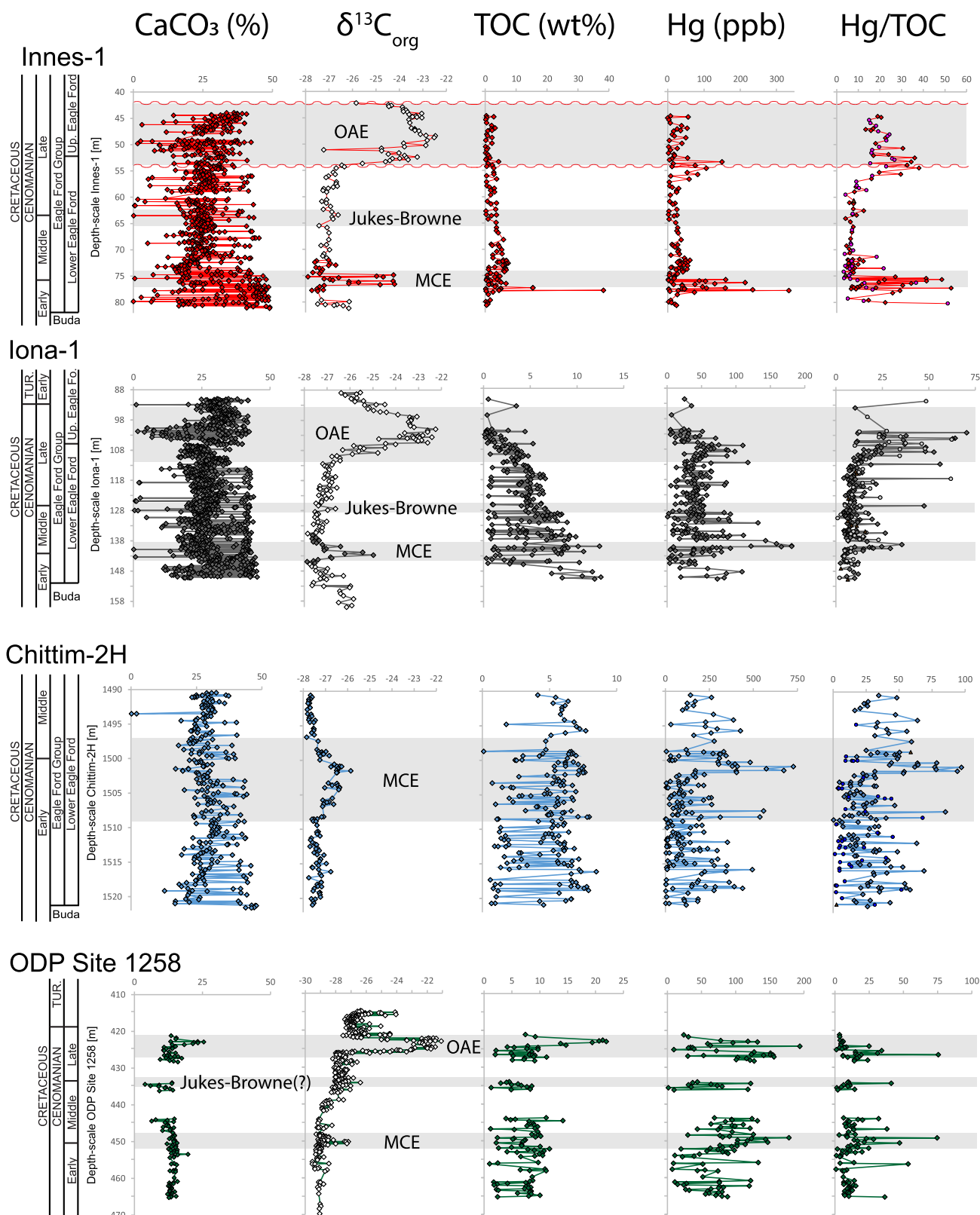


**Figure 2.** Data from the Western Interior Seaway and Demerara Rise: Innes-1, Iona-1, Chittim-2H, and Site 1258. Ca (%) (this study),  $\delta^{13}\text{C}_{\text{org}}$  (‰) (full color markers indicate results from this study; Innes-1 empty markers indicate data from Eldrett et al. (2015a, 2017); Innes-1 undulating red lines indicate unconformity following Eldrett et al. (2017); Iona-1 empty markers indicate data from Eldrett et al. (2014); Site 1258 empty markers indicate data from Erbacher et al., 2005), TOC (wt. %; this study), Hg (ppb; this study), and Hg/TOC (ppb/wt. %; this study; circle markers indicate limestones, diamond markers indicate marlstones, and triangle markers indicate bentonites).



Valanginian, Early Aptian, and end-Cretaceous global environmental perturbations, with Hg spikes linked to the Siberian Traps, the Central Atlantic Magmatic Province, the Karoo-Ferrar igneous province, the Parana-Etendeka province, the Ontong-Java Plateau, and the Deccan Traps, respectively (e.g., Charbonnier et al., 2017; Charbonnier & Föllmi, 2017; Grasby et al., 2013; Percival et al., 2015, 2016, 2017; Sanei et al., 2012; Sial et al., 2013; Thibodeau et al., 2016). End-Ordovician Hg enrichments have also been postulated to be evidence for volcanic activity of an as-yet-unidentified Palaeozoic LIP (Gong et al., 2017; Jones et al., 2017). Mercury is strongly enriched in volcanic emissions, which are one of the major natural sources of Hg to the troposphere and stratosphere (Pyle & Mather, 2003). Volcanic Hg is mostly emitted as gaseous elemental mercury (GEM) with other forms of gaseous Hg and particulate Hg representing a minor component (Baginato et al., 2007; Witt et al., 2008). The atmospheric residence time of GEM is 0.5–2 years (Lindqvist & Rodhe, 1985), significantly longer than many other volcanic metals emitted as aerosols and particles, which typically have residence times on the order of a few weeks (Hinkley et al., 1999; Jaenicke, 1980; Mather et al., 2003; Schroeder & Munthe, 1998). Volcanic Hg therefore has a greater likelihood of global dissemination in the atmosphere than most other volcanic trace metals. In modern marine environments, direct atmospheric deposition is the primary source of Hg input (Mason et al., 2012). Riverine discharge, mobilization from sediments, groundwater, and submarine hydrothermal inputs constitute smaller fluxes and can be dispersed in plumes 10s to 100s km in lateral extent, with their size and shape dependent on the prevailing oceanic currents (Bowman et al., 2015; Mason et al., 2012). At the present day, Hg plumes related to mid-ocean ridges can act as a significant source of Hg to the oceans, albeit with a much more limited geographical spread compared to atmospheric mercury (Bowman et al., 2015).

Once mercury has entered the ocean a number of biotic and abiotic processes may affect it, often resulting in the formation of organic-Hg complexes. Consequently, mercury is typically adsorbed onto organic matter when deposited in sediments. In modern environments, this relationship results in a roughly constant Hg/TOC ratio all else being equal (Benoit et al., 2001; Gehrke et al., 2009; Liu et al., 2012; Outridge et al., 2007; Ruiz & Tomiyasu, 2015). In sulfide-rich waters, the precipitation of Hg-sulfide complexes may result in rapid burial of Hg on a scale of weeks to months (Benoit et al., 1999; Niessen et al., 2003).

Here we examine Hg concentrations in sedimentary successions spanning the Mid-Cenomanian to Early Turonian interval, to further constrain the role of LIP volcanism in initiating climatic and oceanographic change during the MCE and the Cenomanian-Turonian OAE 2. To this end, we present the first Hg data for this time interval, from three sedimentary archives in the Southern Western Interior Seaway and one in the equatorial North Atlantic Ocean (Demerara Rise). We compare the Hg/TOC data with published neodymium-isotope data ( $\epsilon\text{Nd}(t)$ ) from Demerara Rise and osmium-isotope data ( $^{187}\text{Os}/^{188}\text{Os}$ ) from the Vocontian Basin, NW Tethys Ocean, as well as with palaeoceanographic models reconstructing dominant palaeocurrent directions. We use these various lines of evidence to assess the most likely volcanic source of the Hg, its timing and its mode of transport.

## 2. Geological Setting

We present data from samples from four marine mudstone successions spanning the Mid-Cenomanian to Early Turonian interval. Three of the sequences are cores (Innes-1, Iona-1, and Chittim-2H) which sample the Eagle Ford Group (Boquillas Formation) in the Southern Western Interior Seaway (Maverick Basin, Texas, USA, Figure 1). The sequences comprise meter-scale marlstone-limestone couplets deposited in a distal, clastic-sediment starved, intrashelf basin along the retro-arc foreland basin of western North America (with a suggested palaeowater depth of ~50–100 m) (Denne et al., 2014; Eldrett et al., 2014, 2015b, 2017; Lowery et al., 2014; Minsini et al., 2017; Pessagno, 1969). Bentonites occur commonly throughout the sedimentary succession of the Western Interior Seaway cores (Eldrett et al., 2014; Figure 2). These layers are thought to represent geologically instantaneous massive Plinian eruptions from the Western Cordilleran convergent margin. This margin is a known site of abundant Late Cretaceous felsic magmatism that resulted in intrusive batholiths and plutons (e.g., Allmendinger, 1992; Bird, 1998; Burchfiel & Lipman, 1992; Desmares et al., 2007; Dickinson & Lawton, 2001), as well as extrusive features that injected 10s to 100s km<sup>3</sup> of ash into the atmosphere (Sellards et al., 1932). This ash was transported downwind to the east and eventually covered large portions of North America and the adjacent oceans (e.g., Allmendinger, 1992; Burchfiel & Lipman, 1992; Sellards et al., 1932). The bentonites typically form thin beds (mm to m thick; average ~4 cm) correlatable for

100s to 1,000s km (Eldrett et al., 2015a) and their contacts tend to be sharp although biological and current reworking have led to some modification.

The fourth core (from ODP Site 1258) is located on the northwest-facing slope of the Demerara Rise, off Suriname (South America, Figure 1), where the sediments were deposited at the southern edge of the proto-North Atlantic Ocean, a semienclosed basin with its long axis roughly perpendicular to the direction of the persistent trade winds (Trabucho Alexandre et al., 2010). The proto-North Atlantic was connected to the Pacific Ocean through the Central American Seaway, which separated North and South America (Figure 1). The stratigraphy of this core is represented by laminated high-TOC mudstones, characterized by TOC values of 5–10% (and up to 29% around the OAE 2 level), phosphatic nodules, and well-preserved fish-debris (Erbacher et al., 2005; Friedrich et al., 2006, 2009; Hetzel et al., 2009).

### 3. Analytical Methods

#### 3.1. Mercury Analyses

Sedimentary mercury concentrations (Figure 2) were measured using  $50 \pm 5$  mg of powdered sample with a Lumex RA-915 Portable Mercury Analyzer coupled to the PYRO-915 Pyrolyzer (as described by Bin et al., 2001). Fifteen peat-standard samples (NIMT/UOE/FM/001—Inorganic Elements in Peat) with a Hg concentration of  $169 \pm 7$  ppb, were used to calibrate the Lumex prior to each run and to estimate external reproducibility. Mercury concentrations were then subsequently normalized against % TOC to correct for the efficient complexation of Hg to organic matter.

#### 3.2. Organic-Carbon-Isotope Analyses ( $\delta^{13}\text{C}_{\text{org}}$ )

Previous studies on the Innes-1 and Iona-1 cores generated well-defined  $\delta^{13}\text{C}_{\text{org}}$  records for OAE 2, but only low-resolution signatures across the Mid-Cenomanian Event (MCE) (Eldrett et al., 2014, 2015a, 2017). Additional measurements were undertaken to increase the data resolution across the MCE interval for these cores (Figures 2 and 3). Furthermore, a new  $\delta^{13}\text{C}_{\text{org}}$  curve is presented from the Chittim-2H core. This core was drilled and recovered from the central part of the Maverick Basin and records the MCE in a more expanded section than those in the Innes-1 and Iona-1 cores. Sample density in these three cores varies between 10 and 20 cm. One gram aliquots of homogenized sample powder were decarbonated with 40 mL cold 3M HCl and were subsequently rinsed four times with distilled water to reach neutral pH. About 1–15 mg, depending on TOC concentration, of oven-dried and powdered decarbonated sample residue was weighed into  $8 \times 5$  mm tin capsules for  $\delta^{13}\text{C}_{\text{org}}$  analyses. The analyses were performed at the Stable Isotope Laboratory at the Open University, Milton Keynes using a Thermo Flash HT elemental analyzer coupled to a ThermoFinnigan MAT 253. Accuracy of carbon-isotope ratios on the Vienna Pee Dee Belemnite (VPDB) scale were ensured by applying a three-point calibration using IAEA-CH-6 sucrose, NIST8573 glutamic acid, and IR-041 alanine. The reproducibility determined from these standards was  $<0.1\%$  (1 S.D.,  $n = 23$ ).

#### 3.3. Rock-Eval and Coulomat TOC Analyses

Total carbon (TC) and total inorganic carbon (TIC) were determined for samples from Site 1258 with a Strohlein Coulomat 702 Analyzer (Figures 2 and 3; see details in Jenkyns, 1988). For TC and TIC analyses, sample aliquots were measured, with one aliquot having been heated overnight at 450°C to remove organic matter. Total organic carbon (TOC) was calculated as the difference between TC and TIC. The long-term average value and reproducibility of TOC measurements on the in-house SAB134 standard is  $2.95 \pm 0.14$  wt. % (2 S.D.,  $n = 27$ ).

For all remaining Eagle Ford samples (cores Innes-1, Iona-1, and Chittim-2H), TOC was measured by Rock-Eval pyrolysis on a Rock-Eval VI standard instrument with pyrolysis and oxidation ovens. Laboratory procedures as described in Behar et al. (2001) were used. Quality control was provided by an in-house SAB134 standard and the certified IFP160000 standard, which were regularly run between samples. The reproducibility of TOC analyses of the in-house SAB134 and the reference IFP160000 standards are, respectively,  $\pm 0.22\%$  and  $\pm 0.08\%$  (2 S.D.). The long-term average TOC values of SAB134 standard and IFP160000 are 2.98% and 3.27%, respectively.

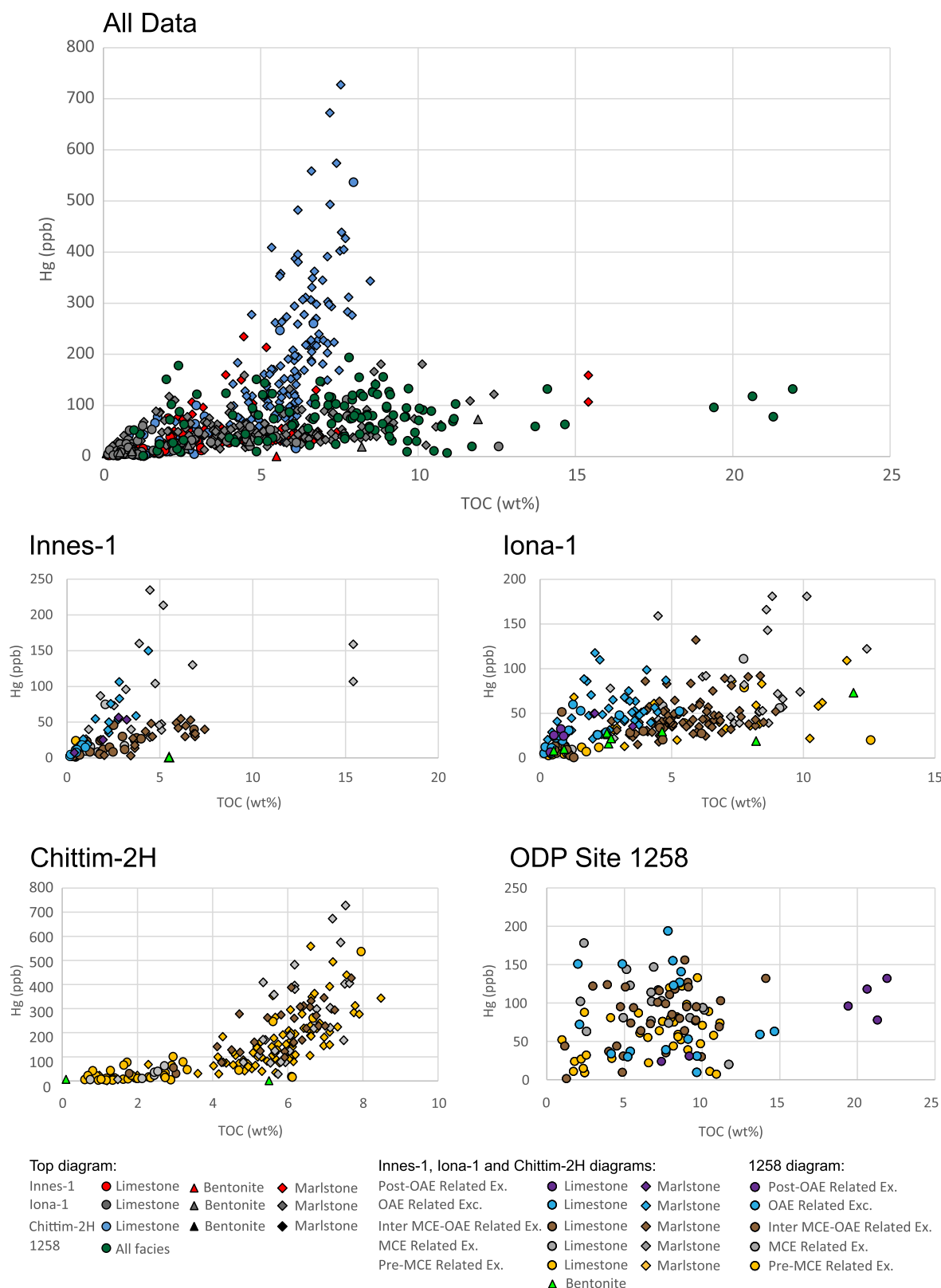


**Figure 3.** Data from the Western Interior Seaway and Demerara Rise plotting Hg (ppb) against TOC (wt. %). Top figure shows data from Innes-1, Iona-1, Chittim-2H and ODP Site 1258. Bottom four figures show Hg (ppb) against TOC (wt. %) for each individual core and separated for the stratigraphic intervals spanning the Pre-MCE, MCE, Inter-Excursion Period, OAE 2, and Post-OAE 2.

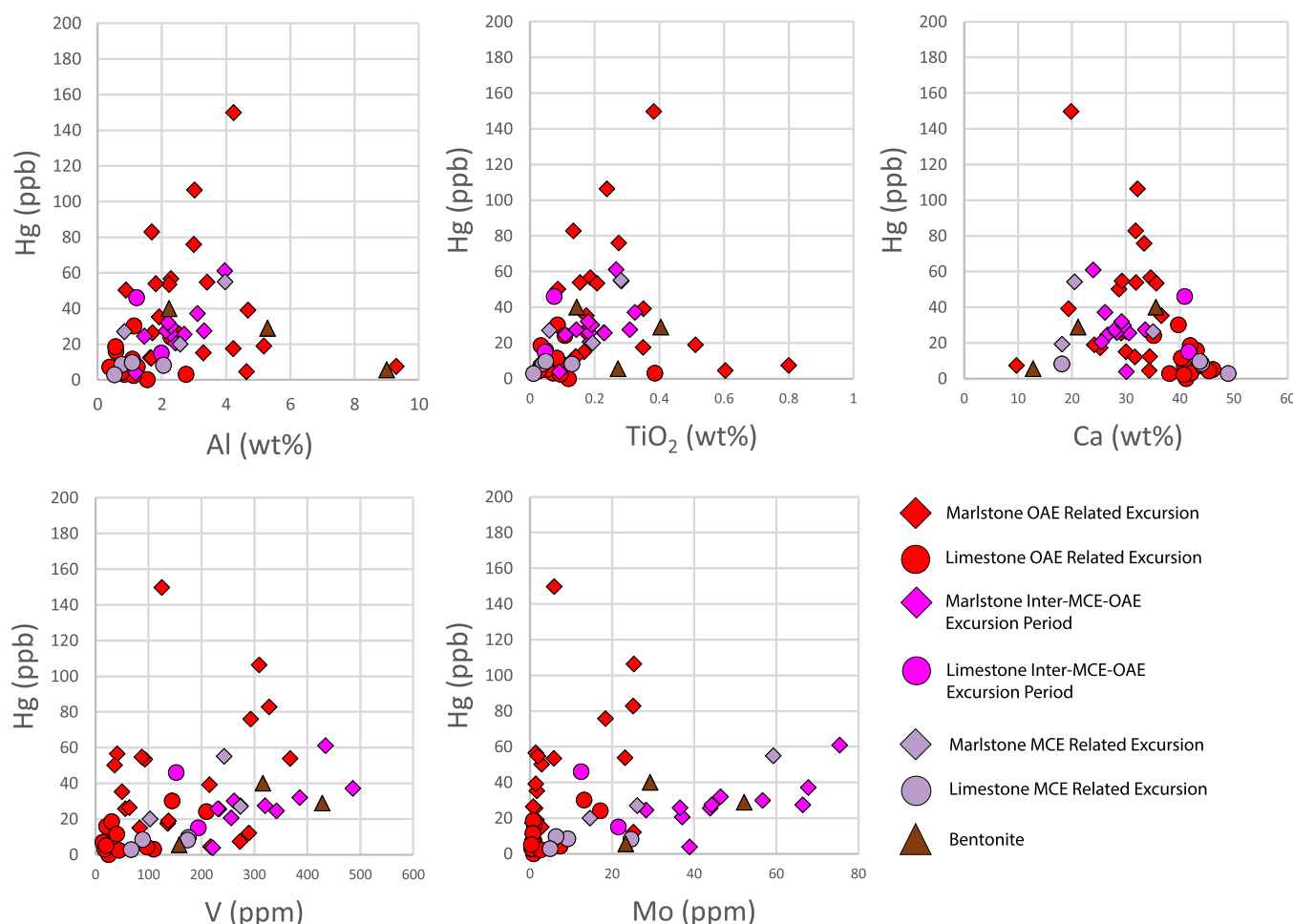


**Figure 4.** Data from Innes-1 showing cross-plots between Hg (ppb; this study) and Al, TiO<sub>2</sub>, Ca, V and Mo (Eldrett et al., 2017). Data are split following three stratigraphic intervals spanning the MCE, OAE 2, and the Inter-Excursion Period.

### 3.4. ICP-MS

New samples were analyzed for major elements and trace metals using Inductively Coupled Plasma Mass Spectroscopy (ICP-MS) and Optical Emission Spectroscopy (OES) at Chemostrat Ltd., UK. To evaluate the redox state (Figure 4), the concentrations of redox-sensitive trace metals were determined, in particular, molybdenum (Mo) and vanadium (V), both of which have been widely used to infer paleoredox conditions in modern and ancient sediments (Algeo & Rowe, 2012; Brumsack, 2006; Tribovillard et al., 2006). These redox-sensitive trace metals show variable solubility with redox state, resulting in authigenic enrichments in oxygen-depleted sedimentary environments. To investigate the influence of changing detrital input, aluminium (Al) and titanium oxide (TiO<sub>2</sub>) were used to normalize the data (Figure 4), as they are commonly utilised as a proxy for terrigenous detrital material due to their relative chemical inertness and lack of biological uptake (Algeo & Rowe, 2012; Brumsack, 2006; Tribovillard et al., 2006).

## 4. Results

### 4.1. New Carbon-Isotope Stratigraphy of the MCE

The  $\delta^{13}\text{C}_{\text{Org}}$  isotope record of Chittim-2H is characterized by an overall positive isotopic excursion (1508.3–1496.2 m) containing two key positive excursions of circa 1.3‰ (1505.77–1503.28 m) and 1.4‰ (1503.28–1499.37 m), reflecting MCE 1a and 1b (Figure 2). The  $\delta^{13}\text{C}_{\text{Org}}$  isotope record of Innes-1 is characterized by a series of positive excursions (between 77.51 and 72.19 m) specifically two key excursions of circa 1.9‰ (at ~76.63 m) and 2.1‰ (at ~74.89 m), also reflecting MCE 1a and 1b. The previously published data of Iona-1



(Eldrett et al., 2015a) are similar to the new Innes-1 data, with two clear positive excursions of 1–1.5‰ at 142.71 m and 139.86 m which could be interpreted as MCE 1a and 1b, respectively. Further to this, these chemostratigraphic markers match the previously published biostratigraphy of Innes-1 and Iona-1, where the positive CIE of the MCE of both cores are bracketed by the highest occurrence of *Rotalipora brotzeni* and the lowest occurrence of *Helvetoglobotruncana praehelvetica* (Eldrett et al., 2015a, 2017).

#### 4.2.1. Hg/TOC: Eagle Ford

##### 4.2.1.1. Hg/TOC: Eagle Ford MCE Excursion

All three Western Interior Seaway cores show evidence of Hg and Hg/TOC excursions around the same stratigraphic level as the MCE. Chittim-2H, shows the largest Hg/TOC excursion in terms of absolute Hg/TOC magnitude, beginning at 1503.91 m and continuing up to ~1499.95 m (Figure 2). However, it should be noted that these values are above a baseline outside the MCE level stratigraphy with relatively scattered data points. At Chittim-2H the Hg/TOC ratio values reach highs of 94, 97, and 78 ppbHg/wt. % TOC at 1500.26, 1500.89, and 1501.45 m, respectively, and the Hg/TOC ratios remain greater than 20 ppbHg/wt. % TOC between 1502.12 and 1499.95 m.

Innes-1 shows the second largest MCE-related Hg/TOC excursion in terms of absolute Hg/TOC magnitude, occurring from 79.63 to 75.09 m with highs of 53, 30, 36, 41, 48, 41, and 27 ppbHg/wt. % TOC occurring at 77.51, 77.1, 76.63, 76.28, 75.96, 75.74, and 75.46 m, respectively (Figure 2). Between each relative maximum, Hg/TOC values drop by, on average, 17 ppb Hg/wt. % TOC, giving this excursion a slightly scattered appearance. Although low TOC values lead to some spikes in Hg/TOC below the sediments associated with the MCE, at 75.09 m Hg/TOC values drop to 5 ppb Hg/wt. % TOC and remain predominantly lower than 20 ppb Hg/wt. % TOC up to the level of the OAE-2 Hg/TOC excursion (section 3.2.1.2).

Iona-1 records the smallest MCE-related Hg/TOC excursion of the three studied cores in the southern Western Interior Seaway, beginning at ~141 m and continuing up to 135.7 m. Maximum values of 29, 36, and 23 ppb Hg/wt. % TOC are reached at 140.2, 139.0, and 137.4 m, respectively. Between 139.8 and 137.8 m Hg/TOC values remain above 20 ppbHg/wt. % TOC. Prior to the MCE Hg/TOC excursion, Hg/TOC values remain lower than 12 ppbHg/wt. % TOC. Above the MCE-related Hg/TOC excursion, in the interval between the MCE and OAE 2, the signal is more erratic than Innes-1 with at least 2 Hg/TOC spikes >30 ppbHg/wt. % TOC.

##### 4.2.1.2. Hg/TOC: Eagle Ford OAE 2 Excursion

Although the Iona-1 Hg/TOC signal shows a degree of scatter, both Innes-1 and Iona-1 contain Hg and Hg/TOC excursions which precede and continue through part of the positive CIE of OAE 2 (Figure 2; see section 3.2.1.3). Iona-1 shows a number of large Hg/TOC excursions beginning at ~112.6 m and persisting up to ~101.6 m (Figure 2). Over this 11 m section there are six noteworthy peaks: at 112.4, 108.4, 107, 105.6, 104, and 102.2 m, which reach Hg/TOC ratios of 56, 53, 49, 46, 63, and 71 ppbHg/wt. % TOC, respectively. Between each of these excursions Hg/TOC ratio values decrease to less than 15 ppb Hg/wt. % TOC. Stratigraphically above the OAE 2 interval there are few data points, but Hg/TOC ratios generally decrease to less than 10 ppb Hg/wt. % TOC.

Innes-1 shows a slightly smaller Hg/TOC excursion than Iona-1, which extends from ~56.6 to ~47.2 m (Figure 2). Hg/TOC values increase from ~8 in the interval below OAE-2, remain generally higher than 20 between 55.35 and 52.13 m, and reach highs of 30, 38, 32, 34, 36, and 30 ppb Hg/wt. % TOC at 55.74, 54.55, 54.22, 53.33, 52.6, and 50.77 m, respectively. Above OAE-2, Hg/TOC ratios decrease to ~13 ppb Hg/wt. % TOC, rising to ~20 from 47.1 m to the 44.62 m.

##### 4.2.1.3. Hg/TOC: Eagle Ford Hg/TOC lag

The Hg/TOC excursions in the Iona-1 and Innes-1 cores appear to display contrasting behavior in terms of their stratigraphic relationships with the MCE-related CIEs. The Hg/TOC excursion in Iona-1 occurs ~4.9 m stratigraphically up-section from the onset of the corresponding CIE, whereas the onset of the MCE-related Hg/TOC excursion in Innes-1 precedes the onset of the CIE by up to 2.8 m of stratigraphy (Figure 2). These relationships indicate a significant offset between the start of the Hg/TOC excursions in the Innes-1 and Iona-1 cores.

With regard to OAE 2, the onset of the Hg/TOC excursions in both Innes-1 and Iona-1 stratigraphically precede the CIE by ~2 m and ~4 m, respectively, with the Hg/TOC excursions of both cores beginning at the same stratigraphic level. It should be noted that the irregularly defined Hg/TOC baseline between the MCE and OAE 2 in the Iona-1 core data complicate definition of the exact offset. Identification of the Hg/TOC

versus CIE offset in the Innes-1 core is complicated by a stratigraphic unconformity at ~54 m in Innes-1 (Eldrett et al., 2017).

#### 4.2.1.4. Hg/TOC: Eagle Ford Baseline

Prior to the MCE-related Hg/TOC excursion, between 80.6 and 79.63 m, Innes-1 has relatively high Hg/TOC values, with 50% of data points over 20 ppb Hg/wt. % TOC with a single high data point of 51 ppb Hg/wt. % TOC recorded at 80.6 m (Figure 2). Between the top of the MCE Hg/TOC excursion and the base of the OAE-2 Hg/TOC excursions at 75.09 and 55.6 m values remain below 20 ppbHg/wt. % TOC, with the vast majority of values falling in the range 5–10 ppb Hg/wt. % TOC (Figures 2, 3, and 5).

In the Iona-1 core, Hg/TOC values remain consistently lower than 12 ppb Hg/wt. % TOC below the MCE. Stratigraphically, between the levels recording the end of the MCE and onset of the OAE, Hg/TOC shows increases at 135.7 and 112.6 m. Here the curve is more erratic with data points at 135.2, 132.2, 126.2, 123.4,

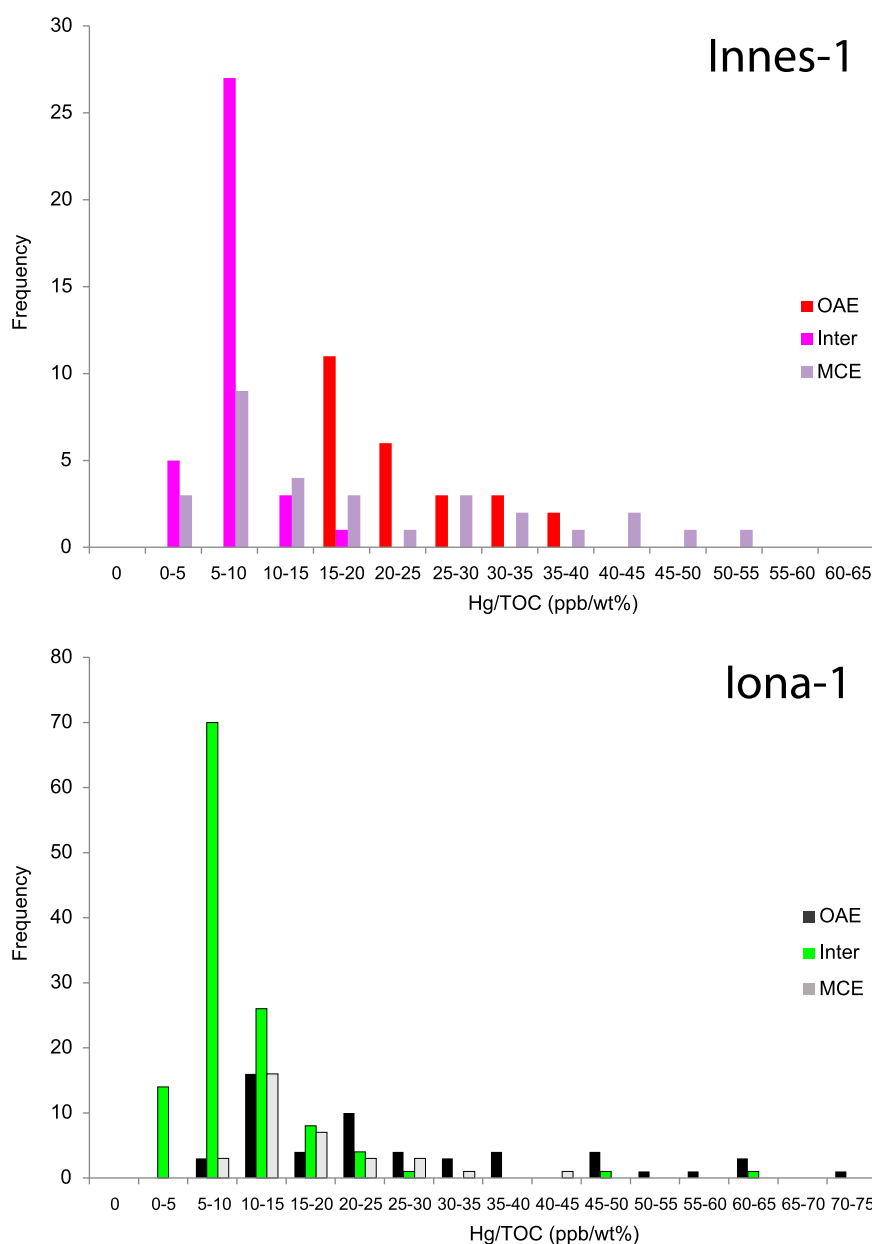


**Figure 5.** Histograms of the number of samples, from the Innes-1 and Iona-1 cores, occurring per succeeding bin of 5 ppbHg/wt. % TOC class widths. Data have been split following the stratigraphic intervals spanning the MCE, OAE 2, and the Inter-Excursion Period.

119.9, and 117.2 m reaching 26, 22, 48, 24, 22, and 62 ppb Hg/wt. % TOC, respectively (Figure 2). However, 70% of Hg/TOC values remain below 10 ppb Hg/wt. % TOC and 90% remain below 15 ppbHg/wt. % TOC (Figure 5).

The Hg/TOC curve of Chittim-2H has the most scattered data of the three cores. Stratigraphically above and below the MCE, Hg/TOC values continuously jump between >40 ppb Hg/wt. % TOC and <15 ppb Hg/wt. % TOC. A number of high Hg/TOC values are found at 151.82, 1511.84, 1508.18, 1507.3, 1498.7, 1497.2, 1495.7, and 1494.13 m with values of 69, 63, 68, 86, 59, 59, 56, and 64 ppbHg/wt. % TOC, respectively, and lows of 5, 14, 5, 9, 10, 25, 31, 17, and 16 recorded in intervening levels (Figure 2).

#### 4.2.2. Hg/TOC: Demerara Rise (ODP Site 1258)

##### 4.2.2.1. Hg/TOC: Site 1258 MCE Excursion

High and variable Hg/TOC values occur stratigraphically below and above the MCE level. Superimposed on the background variability, the Site 1258 data are suggestive of a well-defined Hg/TOC excursion from 452.39 to 448.59 m, coinciding with the MCE positive CIE. Hg/TOC peaks of 47 and 75 ppb Hg/wt%TOC occur at 450.59 and 449.18 m; between these peaks Hg/TOC values drop to 14 ppb Hg/wt. % TOC (Figure 2). The overall peak values occur in direct concert with a shift to more radiogenic  $\epsilon\text{Nd}(t)$  values (Figure 6, Jiménez-Berrocso et al., 2010; Macleod et al., 2008; Martin et al., 2012).

##### 4.2.2.2. Hg/TOC: Site 1258 OAE 2 Excursion

The data from Demerara Rise suggest a Hg/TOC excursion around the OAE 2 positive CIE, which extends from 426.97 to 423.59 m, reaching Hg/TOC highs at 426.62, 426.16, and 425.52 m of 75, 31, and 34 ppbHg/wt. % TOC, respectively (Figure 2). As with the MCE-related Hg/TOC excursion, peak values occur in direct concert with a shift to more radiogenic  $\epsilon\text{Nd}(t)$  values (Jiménez-Berrocso et al., 2010; Macleod et al., 2008; Martin et al., 2012),  $\sim 0.7$  m below the initiation point of the global positive CIE that characterizes OAE 2 (Figure 6).

##### 4.2.2.3. Hg/TOC: Site 1258 Hg/TOC lag

There is a stratigraphic lag between the peak of the MCE Hg/TOC excursion and the CIE, with peak Hg/TOC values post-dating the onset of the MCE 1b CIE (as defined by Friedrich et al., 2009), by  $\sim 0.8$  m (Figure 2). A stratigraphic lag also exists between the onset of the OAE 2 related Hg/TOC excursion and the onset of the associated positive CIE, the onset of the first preceding the ladder by  $\sim 0.7$  m (Figure 2).

##### 4.2.2.4. Hg/TOC: Site 1258 Baseline

Prior to the MCE, over 95% of the Hg/TOC data points at Site 1258 are below 15 ppbHg/wt. % TOC with only two data points reaching over 20 ppbHg/wt. % TOC. Eighty percent of data points between the MCE and OAE 2 have values less than 15 ppbHg/wt. % TOC and 87% less than 20 ppbHg/wt. % TOC (Figure 2). Three anomalously high points of 38, 31, and 41 ppbHg/wt. % TOC occur at 446.79, 443.98, and 434.38 m, respectively.

Importantly, all Hg/TOC excursions discussed here (sections 3.2.1 and 3.2.2) are based on increases in Hg concentrations and increases in Hg concentrations relative to TOC rather than decreases in TOC.

## 5. Discussion

### 5.1. Hg Versus Major and Redox-Sensitive Trace-Metal Concentrations

Changes in nutrient fluxes to the global ocean can lead to increases in marine primary productivity, which can lead to a greater burial efficiency of exported organic matter, an increase in the preservation of organic matter and also the sequestration of Hg. Associated changes in the redox state of the water column and sedimentary pore waters and especially the development of euxinic,  $\text{H}_2\text{S}$  rich water-column conditions may also result in Hg-sulfide precipitating in marine sediments (Sanei et al., 2012). These processes may have affected the rate of Hg sequestration in the past. In this study, changes in major elements and compounds of detrital sedimentary origin, which possibly broadly reflect changes in nutrient supply from landmasses into the marine realm, show no obvious links to mercury concentrations or their stratigraphic position related to the MCE and OAE 2 CIEs within the Innes-1 core (Figure 4). The increased supply of detritus-related minerals due to an intensified hydrological cycle during the MCE and OAE 2 likely accounts for the generally poor correlation between Hg and Al and  $\text{TiO}_2$  concentrations (Figure 4, Blättler et al., 2011; Erbacher et al., 2001; Pogge von Strandmann et al., 2013; van Helmond et al., 2013). Under anoxic and euxinic conditions higher concentrations of organic matter are preserved due to lower levels of aerobic biological activity in the water column or in the sedimentary pore-space (e.g., Demaison & Moore, 1980). Both

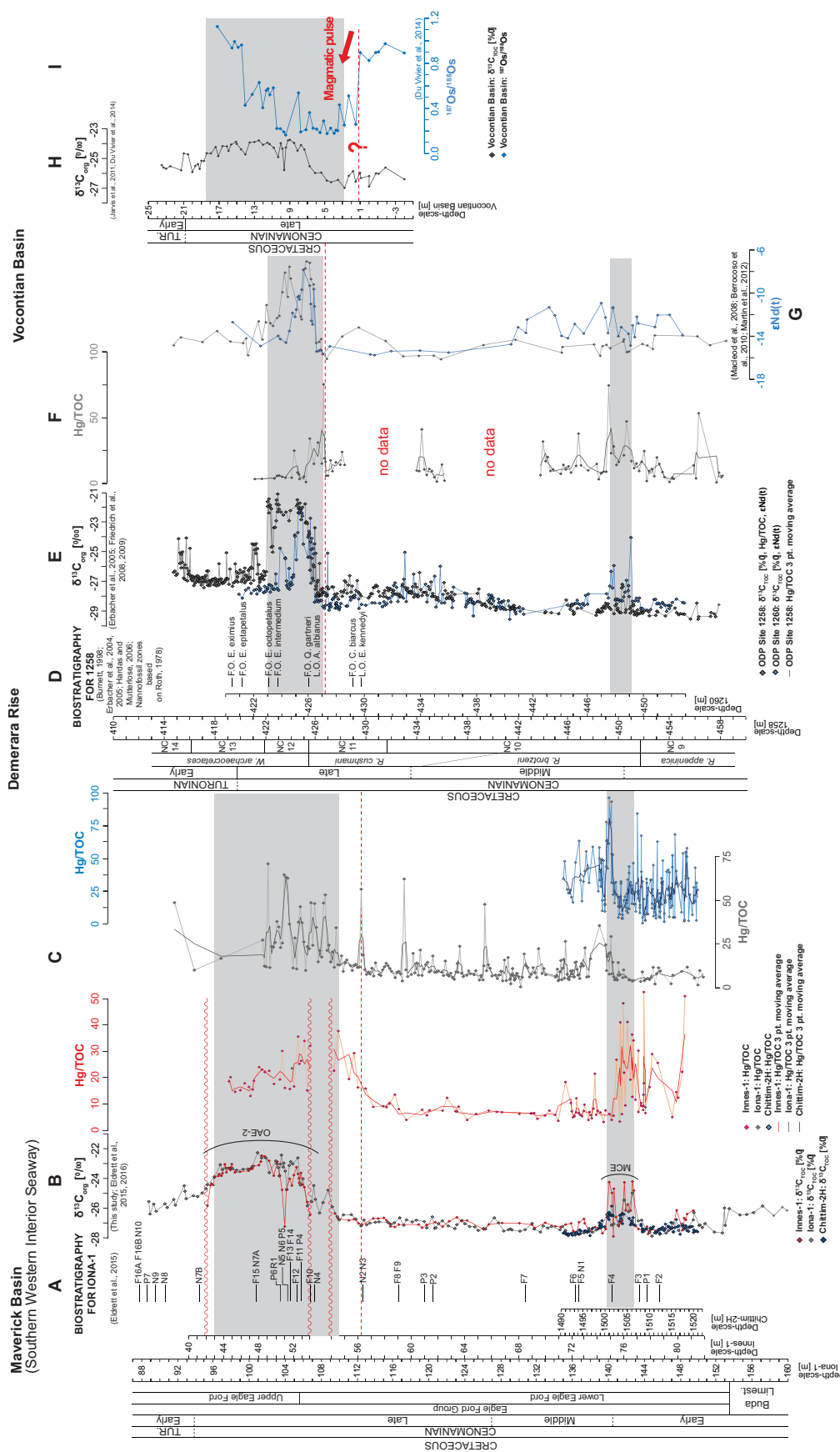


**Figure 6.** Data from the Western Interior Seaway Innes-1, Iona-1, and Chittim-2H cores: (a) Biostratigraphy of the Iona-1 core. Planktonic Foraminifera Events: LO *Rotalipora brotzeni* = F2; LO *Thalmanella appenninica* = F3; FO *Whiteinella aprica* = F4; FO *Helvetoglobotruncana praehelvetica* = F5; FO *Rotalipora cushmani* = F6; FO *Whiteinella archaetretacea* = F7; FO cons. *Rotalipora cushmani* = F8; FO cons. *Whiteinella archaetretacea* = F9; LO *Rotalipora deekel* = F10; LO *Thalmanella greenhornensis* = F11; LO *Rotalipora cushmani* = F12; LO *Thalmanella hagni* = F13; FO *Guembeltia cenomana* = F14; FO *Heterohelix reussi-moremani* ("Heterohelix shift") = F15; FO *Marginothracana schneegansi* = F16a; FO *Marginothracana schneegansi* = F16b. Calcareous Nannoplankton: FO *Corollithion kennedyi* = N1; ACME *Corollithion kennedyi* = N2; FO *Gartnerago obliquum* = N3; LO *Axopodorbabidus albanicus* = N4; LO *Corallithion kennedyi* = N5; LO *Corallithion striatus* = N6; LO *Heleneia chistia* (Iona-1) = N7a; LO *Heleneia chistia* (extrapolated) = N7b; FO *Quadrum gartneri* = N8; FO *Eprolithus octopetalus* = N9; FO *Eprolithus eptapetalus* = N10. Radiolarians: FO *Radiolarians* = R1. Dinoflagellate Cysts: FO *Litosphaeridium siphoniphorum* = P1; LSAO *Boselinia* spp. cf. sp.1 & sp.3 of Praus (2012b) = P2; LCO *Cyclonephelium longispinatum* = P3; FO *Cyclonephelium membraniphorum* = P4; LO *Adnatospaeridium tutulolum* = P5; LO cons. *Litosphaeridium siphoniphorum* = P6; LO *Adnatospaeridium chonetum* = P7. Where LO = last occurrence; LCO = last common occurrence; FO = first occurrence; FCO = first common occurrence; cons. = consistent occurrence. (b) δ¹³C<sub>org</sub> (this study; Eldrett et al., 2015a, 2017; Innes-1 undulating red lines indicate unconformity as adapted from Eldrett et al. (2017), illustrating a split in the Innes-1 depth scale due to a hiatus relative to Iona-1). (c) Hg/TOC (this study). Data from Demerara Rise ODP Sites 1258 and 1260: (d) Biostratigraphy of ODP Site 1258 (Burnett, 1998; Erbacher et al., 2004, 2005; Hadas & Mutterlose, 2006). Nannofossil zones are based on Roth (1978). (e) δ¹³C<sub>org</sub> (Erbacher et al., 2005; Friedrich et al., 2009). (f) Hg/TOC (this study). (g) εNd (Jiménez-Berrosco et al., 2010; Mädel et al., 2008; Martin et al., 2012). Data from the Vocontian Basin: (h) δ¹³C<sub>org</sub> (Jarvis et al., 2011). (i) ¹⁸⁷Os/¹⁸⁸Os (Du Vivier et al., 2014). The red dashed line marks the onset of the ¹⁸⁷Os/¹⁸⁸Os excursion attributed to a magmatic pulse and/or basalt-seawater interaction as recorded in the Vocontian Basin, and possible stratigraphic correlation to the Demerara Rise and Western Interior Seaway sedimentary archives.

Mo and V become enriched under very low oxygen and sulfidic conditions at the sediment-water interface or in the water column (e.g., Algeo & Maynard, 2004; Tribouillard et al., 2005, 2006). Therefore, in low oxygen, aquatic depositional environments where organic matter is accumulating, a positive correlation exists between redox-sensitive trace metal and Hg concentrations and TOC. The Hg concentrations throughout the Innes-1 core are generally lower in CaCO<sub>3</sub>-rich limestone beds, because Hg readily binds with organic compounds and therefore is more enriched in the relatively TOC-rich more marly facies.

The relative distribution of Hg versus redox-sensitive trace elemental concentrations (e.g., Mo and V) varies throughout the Innes-1 core (Figure 4). The OAE 2 interval is marked by relatively low redox-sensitive trace-metal concentrations and relatively high Hg concentrations, whereas the MCE and the interexcursion period between the MCE and OAE 2 show reasonably strong positive correlations between Mo and V and Hg. This pattern can be explained by: (a) strongly enhanced volcanogenic fluxes of Hg during OAE 2 relative to the fluxes of Mo and V into the sedimentary realm, (b) the strong facies control on sedimentary Mo and V concentrations, with predominantly CaCO<sub>3</sub>-rich facies during OAE 2 in the Innes-1 core resulting in low Mo and V values (less than 30 ppm V and less than 10 ppm Mo), (c) globally reduced Mo and V seawater concentrations during the MCE and OAE 2 due to global trace metal drawdown and the associated depletion of the marine trace-metal inventory, under conditions of expanding oxygen-depletion in geographically widespread regions (Eldrett et al., 2017; Hetzel et al., 2009; van Bentum et al., 2009; Jenkyns et al., 2017), and (d) relatively reduced sedimentary Mo and V concentrations throughout OAE 2 (Figure 4) due to a basinal oxygenation event related to open water-mass exchange (Eldrett et al., 2014, 2017).

## 5.2. MCE and OAE 2 Hg/TOC Excursions

Previous studies investigating Hg enrichments during global climatic perturbations have used such data to connect the events to LIP volcanism (section 1). The four cores studied here show elevated Hg and Hg/TOC values in sediments deposited during the MCE and OAE 2. LIP volcanism (coeval LIPs shown in Figure 1) has been suggested as the initial trigger for the climatic and palaeoceanographic perturbations associated with OAE 2 (see section 4.2, Du Vivier et al., 2014, 2015; Jenkyns et al., 2017; Orth et al., 1993; Snow et al., 2005; Tegner et al., 2011; Turgeon & Creaser, 2008). During past major global-change events, an increased flux of mercury to the global ocean-atmosphere system could also have been achieved by widespread wildfires, large-scale volcanism, release of thermogenic Hg from volcanism, or a bolide impact. Evidence for widespread wildfires, thermogenic emissions or subaerial LIP emplacement at the MCE and OAE 2 is, however, lacking (e.g., Alvarez et al., 1984; Kuroda et al., 2007; Pegram & Turekian, 1999; Turgeon & Creaser, 2008), and previous estimates of bolide impacts have suggested they would not provide enough Hg to the atmosphere to result in a significant Hg anomaly (Sial et al., 2014). Therefore the Hg/TOC excursions presented here may be taken as new evidence suggesting a significant flux of volcanically derived Hg and associated gases and (toxic) compounds to the southern proto-North Atlantic (Demerara Rise) and the southern Western Interior Seaway (Maverick Basin) during these periods.

Results from the localities studied here show that Hg/TOC ratios are 10–100 times lower than found in most previous studies of other Mesozoic events (Grasby et al., 2013; Percival et al., 2015; Sanei et al., 2012; Sial et al., 2016; Thibodeau et al., 2016) with the possible exception of OAE 1a (cf. Charbonnier and Föllmi, 2017). There are a number of possible reasons for the differences in the magnitude of MCE and OAE 2 related Hg/TOC ratios described here compared to other Mesozoic events, including: (1) the nature (i.e., subaerial or submarine) and geographical position of the LIP; (2) the intensity, length, and type (e.g. effusive versus explosive) of the volcanic episode(s); (3) thermogenic release of Hg from organic-rich sediments; and (4) muting of Hg/TOC due to high TOC levels and the resulting dampening of Hg/TOC values in the studied sedimentary archives.

(1) The first reason is discussed in the section 4.3 that follows. Each of these other factors is discussed in turn here.

(2) Subaerial LIP volcanism may have resulted in relatively high Hg fluxes directly into the atmosphere, therefore possibly resulting in larger Hg excursions. However, at present the Hg fluxes of past subaerial LIP volcanism are largely unconstrained. Longer and more intense episodes of volcanism might expel more mercury into the ocean-atmosphere system and transfer larger amounts of Hg into the sedimentary realm over shorter periods of time. Differences in past LIP eruption type and their long-term effects on Hg expulsion have not been widely studied, although most LIPs are thought to have been predominantly effusive



with underlying sill and feeder dyke complexes (e.g., Bryan & Ernst, 2008). Bentonites make up around 5% of the Western Interior Seaway cores (>300 occurrences in Iona-1: Minisini et al., 2017) and are probably derived mostly from explosive silicic caldera eruptions. The bentonites measured here show low Hg/TOC ratios of between 5 and 15 ppbHg/wt. % TOC, values comparable to the generally low sedimentary background values in the Innes-1 core (Figures 2 and 3). Furthermore, the strata above and below the bentonites do not appear to be geochemically impacted by proximity to these deposits (see supporting information Figures) as the underlying and overlying sediments display values comparable to sediments in other parts of the core. Hence, it is unlikely that the Hg in our study area is sourced from the Western Cordilleran convergent margin or that Hg migrated from the bentonites. Therefore, Hg has not become diagenetically enriched in underlying and overlying sediments.

(3) The thermogenic release of Hg due to the intrusion of dykes and/or sills into organic-rich strata could potentially release large fluxes of Hg to the ocean-atmosphere system due to its volatility. This mechanism has been suggested for other global-change events, such as the Toarcian Oceanic Anoxic Event (T-OAE) where dykes and sills from the Karoo-Ferrar LIP are known to have penetrated organic-rich sedimentary basins (Percival et al., 2015). It is possible that one of the LIPs known to be active during OAE 2 period included magmas which intruded organic-rich sediments. However, there is no current evidence for thermogenic emissions during OAE 2 and further work is required to assess and quantify the likely effect of this mechanism.

(4) As TOC contents in the Maverick Basin are highest before and after the MCE and then gradually drop to lower values around OAE 2 (Figure 2) it is unlikely that high levels of organic matter resulted in a muting effect.

In summary, it may be reasonable to suggest that the most likely cause of the observed increases in sedimentary Hg and Hg/TOC was LIP volcanism and its nature and its proximity to the here studied sedimentary archives during deposition.

### 5.3. Submarine LIPs and Hg Dispersal Mechanism

Submarine magmatic activity and associated basalt-seawater interaction has been suggested as the initial trigger for the climatic and palaeoceanographic perturbations associated with OAE 2 (i.e., Courtillot & Renne, 2003; Jenkyns et al., 2017; Rampino and Strothers, 1988; Turgeon & Creaser, 2008). A globally observed shift in the  $^{187}\text{Os}/^{188}\text{Os}$  ratio of organic-rich mudstones, to unradiogenic values (du Vivier et al., 2014, 2015; Turgeon & Creaser, 2008), and a change in seawater strontium-isotope ratios to less radiogenic values coinciding with OAE 2, supports this interpretation (Jones & Jenkyns, 2001). Equivalent negative excursions in lithium and calcium isotope ratios during OAE 2, taken to represent changes in seawater values, imply increases in weathering of silicates (Blättler et al., 2011; Pogge von Strandmann et al., 2013), which may indicate subaerial basalt emplacement followed by weathering of an exposed landmass in addition to alteration of submarine basalts.

Of the four LIPs thought to have been active throughout the Cenomanian and Turonian (Figure 1) the only potentially direct evidence that links OAE 2 with the Caribbean Plateau and/or Madagascar (subaerial) Flood Basalt is based on lead-isotope signatures (Kuroda et al., 2007): it should be noted that this study did not incorporate data from the High Arctic and Ontong Java LIPs). The Madagascar LIP has been  $^{40}\text{Ar}/^{39}\text{Ar}$  (Storey et al., 1995) and U-Pb (Torsvik et al., 1998) radioisotopically dated to have formed between  $91.6\text{--}83.7 \pm 0.2\text{--}0.6$  Ma, significantly later than the onset of OAE 2 (although the volcanic basement of the extensive submarine Madagascar Ridge (remains unsampled and undated). The initiation of OAE 2 does correspond well with  $^{40}\text{Ar}/^{39}\text{Ar}$  radio-isotopic ages for the Caribbean LIP ( $95.1$  Ma to  $92.2 \pm 0.46\text{--}0.78$  Ma (Snow et al., 2005), although paired U-Pb analysis is still required to rule out potential bias of the  $^{40}\text{Ar}/^{39}\text{Ar}$  dates toward a younger age due to postdepositional alteration or overprinting by a younger metamorphic event.

Therefore, submarine LIP emplacement during the MCE and OAE 2 may represent a source for elevated oceanic Hg concentrations. Such a mechanism could have featured intense release of hydrothermal Hg during rapid emplacement of mafic rocks, similar to that observed on mid-ocean ridge systems today; potentially accompanied by additional Hg-rich fluids expelled during subsequent basalt-seawater interactions. As mercury has a short (<1 kyr) residence time in the modern ocean compared to other volcanically derived trace metals, it might be expected that sites located more distally from a LIP would show less sedimentary

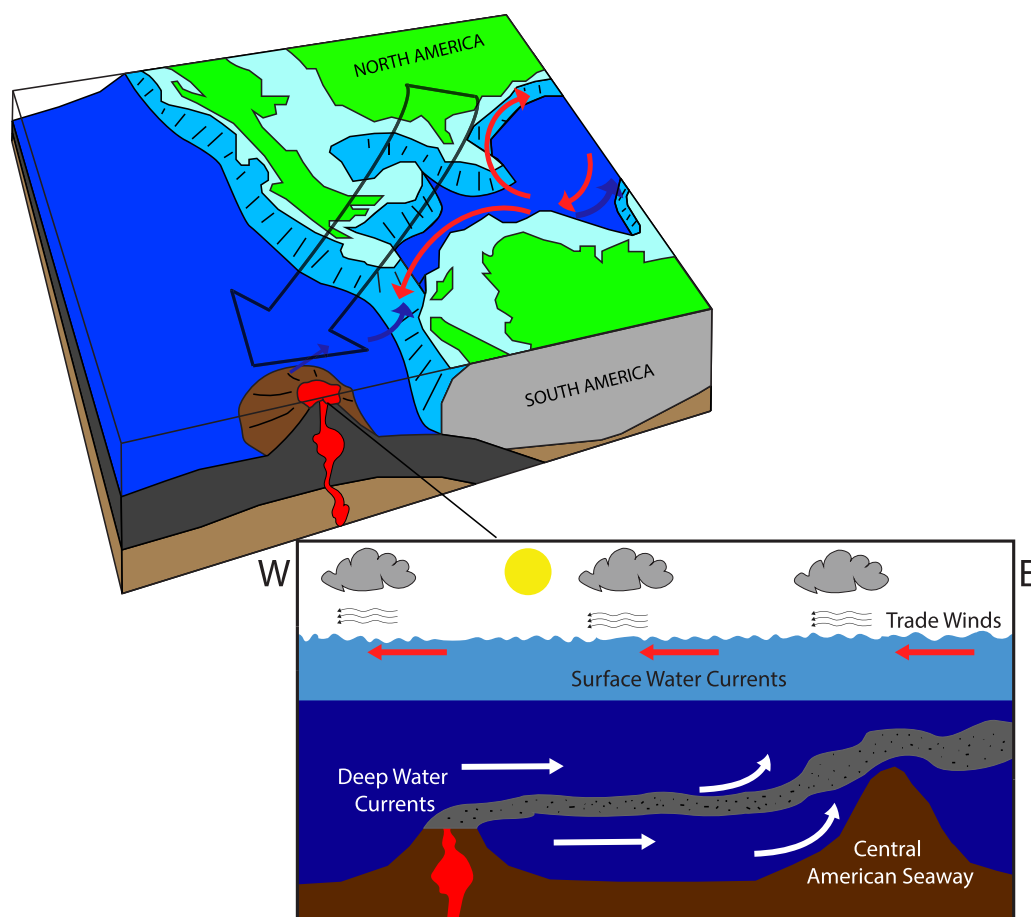


**Figure 7.** Palaeoceanographic model of the Cenomanian-Turonian Pacific and Atlantic Oceans and Western Interior Seaway, showing reconstructed palaeocurrents in the proto-North Atlantic region (modified from Trabucho Alexandre et al., 2010). The trade winds (largest arrow) are credited with causing a dominant westward surface-water flow and circulation (red arrows) leading to upwelling on the southern margins of the Western Interior Seaway. (bottom figure) Schematic diagram showing intermediate/deep waters entering the proto-North Atlantic Basin, acting as a possible conduit for Hg-enriched water masses.

enrichment in Hg than those in more proximal positions. In such a situation, the amount and pattern of sedimentary Hg enrichments observed at any location would have depended on the direction and intensity of the palaeo-ocean currents transporting Hg from source to sink, in addition to the position of the volcanic center, the flux size and any changes to the global oceanic Hg residence time.

Palaeo-ocean models suggest that the palaeogeography and persistent palaeotrade winds in the south-western proto-North Atlantic resulted in a net flow of surface waters through the Central American Seaway into the Pacific Ocean (Trabucho Alexandre et al., 2010). A subsurface counter current has been suggested to have moved in the opposite direction, entering the western proto-North Atlantic at depth and upwelling along the northern and southern continental margins (Trabucho Alexandre et al., 2010). This subsurface counter current could have acted as a transport mechanism to move Hg-enriched waters from the Pacific Caribbean LIP into the southern Western Interior Seaway and the western and southern proto-North Atlantic (Figure 7). A similar model has recently been proposed to explain the occurrence of enhanced concentrations of mafic trace metals and mafic chromium-isotope signatures in the Western Interior Seaway during OAE 2, which were argued to originate from the Caribbean LIP (Holmden et al., 2016; Orth et al., 1993). This situation is also supported by neodymium-isotope records ( $\epsilon\text{Nd}$ ; Figure 6) for the mid-Cretaceous at Demerara Rise that show a shift from extremely unradiogenic values to more radiogenic values, which are akin to Pacific, Tethyan and eastern proto-North Atlantic signatures, during both the MCE (MCE 1b) and OAE 2 (Jiménez-Berrococo et al., 2010; MacLeod et al., 2008; Martin et al., 2012). A similar, low amplitude shift in  $\epsilon\text{Nd}$  is

also recorded further north in southern England (Zheng et al., 2013), and may represent the northwards propagation of a more diffuse radiogenic water mass. The Hg data presented here may, therefore, tie the timing of environmental changes observed during the MCE and during OAE 2 directly to magmatism associated with the Caribbean LIP via a submarine plume of Hg-enriched intermediate to deeper waters. If correct, sedimentary Hg concentrations at sites located outside of the proto-North Atlantic Ocean and the Western Interior Seaway should exhibit small, or undetectable peaks in Hg consistent with a lack of direct atmospheric Hg dispersal.

Alternatively, periodic incursions by boreal dinoflagellate cyst taxa shown in both Canada and the Eagle Ford Group of the Western Interior Seaway during OAE 2 (Eldrett et al., 2014, 2017; Van Helmond et al., 2016) indicate a southward flow of boreal water and therefore may provide a pathway for a second or alternative mercury source from High Arctic Large Igneous Province. The southerly flow of boreal water at this time may be associated with a more complex oceanographic system whereby a strong cyclonic gyre developed in the central Western Interior Seaway drawing both Tethyan waters northward along the eastern margin and boreal waters southward along the western margin of the seaway (Elderbak & Leckie, 2016; Kump & Slingerland, 1999; Slingerland et al., 1996). Importantly, neither model rules out the possibility of multiple LIPs erupting at the same time influencing the Hg concentration of sediments in our studied locations.

We therefore suggest that the sedimentary Hg enrichments observed during the MCE and OAE 2, in contrast to other Mesozoic OAEs, were sourced from localized Hg plumes in subsurface waters. The alternative suggestion remains that volcanogenic trace metals, including Hg, may have entered the atmosphere through the water-column (Bagnato et al., 2017) or directly by explosive/subaerial volcanic activity associated with submarine LIP emplacement. The release and dissolution of volcanogenic gases within the water column would in turn have resulted in smaller fluxes of Hg entering the global atmosphere than would otherwise have been the case. Such a mechanism could explain the reduced sedimentary Hg and smaller and variable Hg/TOC excursions at the MCE and OAE 2, relative to the signals associated with other Mesozoic global-change events proposed to originate from subaerial LIP emplacement.

Possible evidence against atmospheric dispersal of the signal is the decreasing trend in the magnitude of Hg/TOC ratios along a south-to-north transect of the Western Interior Seaway (Chittim-2H → Iona-1 → Innes-1, respectively; Figures 1 and 2), tentatively explained by decreasing concentrations of mercury in the water column due to the increasing distance from the subaqueous source derived from the Caribbean LIP. The longer atmospheric lifetime of Hg means that such differences would have been significantly less marked had the dispersal mechanism been subaerial. Future studies of other marine, but especially also continental sedimentary records from the proto-North Atlantic region and elsewhere, spanning the Cenomanian-Turonian transition, will help to determine the dominant dispersal pathway for Hg at this time.

Irrespective of the dominant dispersal mechanism for Hg during the MCE and OAE 2, the multiple excursions in Hg and Hg/TOC values at these time intervals, observed in the sedimentary records from four different cores, spread over 2 geographically separated regions, strongly suggests a temporal link between increased magmatic activity and major perturbations in global biogeochemical cycles, climate and the palaeoenvironment at those times.

#### 5.4. Comparisons to OAE 1a

Throughout the Early Cretaceous, the Greater Ontong-Java episode of LIP activity led to the formation of the Ontong-Java, Manihiki, and Hikurangi Plateaus in the Pacific Ocean (e.g., Bottini et al., 2012; Kuroda et al., 2011; Méhay et al., 2009; Tejada et al., 2009). Although the establishment of an exact temporal relationship between OAE 1a and LIP activity remains a major challenge, several lines of evidence, such as age correlations to changes in the marine sedimentary lead isotopic composition, a change in volcanogenic trace-element concentrations and an ~880 kyr interval during OAE 1a marked by an exceptionally unradiogenic Os-isotopic composition of the global ocean, suggest that OAE 1a may have been triggered by the emplacement of the Ontong Java Plateau in the central Pacific Ocean (e.g., Bottini et al., 2012; Erba, 1994; Erba et al., 2015; Larson & Erba, 1999; Jones & Jenkyns, 2001; Kuroda et al., 2011; Méhay et al., 2009; Tarduno et al., 1991; Tejada et al., 2009).

Three coeval sedimentary records from the western Tethyan region, across OAE 1a, which were separated by 100–300 km and which were 4,000–7,000 km away from the Ontong Java Plateau, showed only limited

increases in sedimentary Hg/TOC enrichments (Charbonnier and Föllmi, 2017). These Hg/TOC enrichments were suggested to be partly related to supposed changes in primary productivity, redox conditions and TOC preservation rates. However, increased emission of gaseous  $\text{Hg}^0$  during LIP formation was suggested to be the principal source of increased sedimentary mercury enrichment (Charbonnier and Föllmi, 2017). The sedimentary Hg/TOC values associated with OAE 1a show comparable values to the results for OAE 2 shown in this study and were explained by the muting effects of high sedimentary TOC contents in the studied record (Charbonnier and Föllmi, 2017).

As the emplacement of the Ontong-Java Plateau was largely deep sea submarine (Bottini et al., 2012; Erba et al., 2015; Kuroda et al., 2011; Méhay et al., 2009; Tarduno et al., 1991; Tejada et al., 2009) it is likely to have introduced reactive metals directly into the ocean rather than dispersing particulates and gases predominantly through the atmosphere.

Palaeo-ocean models suggest that the palaeogeography and palaeotrade winds in the Tethys and Pacific oceans resulted in a net flow of waters from the Ontong Java LIP to the proto-North Atlantic in a clockwise fashion (Erba et al., 2015; Hay, 2009). A subsurface oceanic counter current has been suggested to result in upwelling along the western Tethyan margins (Hay, 2009). This counter current could have acted as transport mechanism for the movement of a volcanogenically derived plume from the central Pacific Ontong Java LIP to the sites of these cores in the western Tethys. Alternatively, if the distance from the source was too great for a submarine plume to hold a significant Hg concentration then it may suggest that the Ontong-Java LIP temporarily became periodically emerged, as suggested by the local presence of pyroclastic sediments (Thordarson, 2004), thereby providing an atmospheric dispersal mechanism for Hg.

The deep-submarine and geographic position for the formation of the Ontong-Java Plateau may have therefore impacted mercury distributions in the studied sedimentary records spanning OAE 1a. Similar to OAE 1a, the lower Hg/TOC ratios observed across the MCE and OAE 2, compared to other Mesozoic events, may have resulted from localized submarine Hg plumes or the release and dissolution of volcanogenic gases within the water column resulting in smaller fluxes of Hg entering the global atmosphere, relative to levels observed for continental LIP emplacements at other global-change events.

### 5.5. Minor Cenomanian Carbon-Cycle Perturbations: Jukes-Browne Event

A small positive CIE of  $0.8\text{‰}$  is visible both in Iona-1 between 128.36 and 126.1 m and in Innes-1 between 65.49 and 62.39 m. Within the ODP Site 1258 core on Demerara Rise a period of erratic carbon-isotope fluctuation occurs between 435.34 and 432.66 m. However, between these limits there are three particularly high positive CIEs of around  $0.5\text{‰}$ ,  $1\text{‰}$  and  $0.7\text{‰}$  at 435.11, 434.21, and 432.97 m respectively, which may correspond to the minor CIE found in the Western Interior Seaway cores. The CIEs observed in Iona-1 and at Site 1258 fall within the relatively narrow occurrence-range of the planktonic foraminiferal marker species *Rotalipora cushmani* (Eldrett et al., 2015a, 2017; Tsikos et al., 2004) and the position of the CIE in each core occurs in a similar position within chemostratigraphical and sedimentological constraints (Figures 2 and 6). As such, we hypothesize that these CIEs are equivalent to the Jukes-Browne Event, first recognized in the English Chalk (Jarvis et al., 2006) where it spans the correlative upper *A. jukesbrownei* and the lower *C. guerangeri* zones (Hardenbol et al., 1998), and subsequently in central areas of the Western Interior Seaway (Joo & Sageman, 2014). Consequently, this small positive excursion may provide a marker for the base of the Upper Cenomanian in Innes-1, Iona-1, and 1258. A combined astronomical and geochronological age model for the Iona-1 core calibrates the Jukes-Browne Event (128.36–126.1 m) to between  $95.79$  and  $95.69 \text{ Ma} \pm 0.12 \text{ Ma}$  (Eldrett et al., 2015a) therefore potentially assigning a numerical age to both the *Jukesbrownei*-related CIE and more tentatively the Middle-Upper Cenomanian sub-stage boundary of  $95.79 \pm 0.12 \text{ Ma}$  (Eldrett et al., 2015a).

Anomalously high Hg/TOC values of 48 ppbHg/wt. % TOC and 41 ppbHg/wt. % TOC accompany the Iona-1 and Site 1258 CIEs at 126.2 and 434.38 m, respectively. The CIE of Innes-1 is also accompanied by a Hg/TOC excursion, which although of smaller absolute magnitude (12 ppbHg/wt. % TOC), is significantly higher than the lower stable baseline values in this part of the Innes-1 core (Figure 2). It is possible that these excursions implicate volcanism and the potentially accompanying release of  $\text{CO}_2$  and other greenhouse gases and compounds, and associated changes in global carbon burial rates, as drivers for this relatively minor perturbation to the global carbon cycle. However, the true nature of the observed Hg/TOC excursions at this time, defined only by a single data point, albeit in all three cores, needs further study as it also

coincides with low TOC values (Figure 2). This pattern suggests elevated Hg/TOC values may be to some extent an artefact of a change in the deposition and preservation of organic matter during these periods. If the event were caused by volcanic activity, the much smaller size of the CIE found in all three cores indicates that the volcanic event responsible for it would most likely have been significantly smaller in volume or shorter in duration than those responsible for the geochemical anomalies observed for the MCE and OAE 2.

## 6. Conclusions

New sedimentary Hg concentration data from three sites in the Western Interior Seaway and one from the south-western proto-North Atlantic Ocean (Demerara Rise) contain elevated Hg and Hg/TOC values at the stratigraphic levels of the Mid-Cenomanian Event (MCE) and the Cenomanian-Turonian Oceanic Anoxic Event 2 (OAE 2). Values are, however, muted in comparison to signals found during other Mesozoic intervals marked by OAEs and/or global-change events that are associated with coeval subaerial LIP emplacement. The smaller Hg signals associated with OAE 2 and the MCE possibly resulted from Hg dispersal by a submarine plume, following subaqueous LIP emplacement rather than resulting from atmospheric dispersion. The transmission of this plume by subsurface palaeocurrents moving either from the Pacific, through the Central American Seaway into the south-western proto-North Atlantic Ocean or from the Arctic via the Canadian sector of the Western Interior Seaway are consistent with previous palaeoceanographic reconstructions of water mass movements. This study finds no correlation between the enrichment of redox-sensitive trace metals and the MCE-related or OAE 2-related Hg/TOC excursions. In addition, a possible short-term Hg/TOC enrichment, in tandem with a carbon-isotope excursion, is recognized at the level of the Jukes-Browne Event, occurring stratigraphically in-between the MCE and OAE 2 in the Innes-1, Iona-1, and Site 1258 cores.

## Acknowledgments

We thank and acknowledge Shell International Exploration and Production for funding for this project and for providing access to the Innes-1, Iona-1, and Chittim-2H cores and samples. We also thank Blackbrush Oil and Gas L.P. for providing access to the Chittim-2H core and samples. Furthermore, we thank the International Ocean Discovery Program (IODP) for providing access to core-samples from Site 1258 at Demerara Rise. We would also like to thank the two anonymous reviewers who helped us to improve this manuscript. All data can be found in the supplementary information.

## References

- Algeo, T. J., & Maynard, J. B. (2004). Trace-element behaviour and redox facies in core shales of Upper Pennsylvanian Kansas-type cyclothems. *Chemical Geology*, 206, 289–318. <https://doi.org/10.1016/j.chemgeo.2003.12.009>
- Algeo, T. J., & Rowe, H. (2012). Paleocceanographic applications of trace-metal concentration data. *Chemical Geology*, 324, 6–18. <https://doi.org/10.1016/j.chemgeo.2011.09.002>
- Allmendinger, R. W. (1992). Fold and thrust tectonics of the western United States exclusive of the accreted terranes. In B. C. Burchfiel et al. (Eds.), *The Cordilleran orogen: Conterminous US* (Vol. 2, pp. 583–607). Boulder, CO: Geological Society of America. The Geology of North America.
- Alvarez, W., Alvarez, L. W., Asaro, F., & Michel, H. V. (1984). The end of the Cretaceous: Sharp boundary or gradual transition? *Science*, 223, 1183–1186.
- Arthur, M. A., Schlanger, S. O., & Jenkyns, H. C. (1987). The Cenomanian-Turonian oceanic anoxic event II, paleoceanographic controls on organic matter production and preservation. In J. Brooks & A. Fleet (Eds.), *Marine petroleum source rocks, Geological Society Special Publication* (Vol. 4, pp. 399–418). Oxford, UK: Blackwell.
- Bagnato, E., Aiuppa, A., Parello, F., Calabrese, S., D'alessandro, W., Mather, T. A., . . . Wängberg, I. (2007). Degassing of gaseous (elemental and reactive) and particulate mercury from Mount Etna volcano (Southern Italy). *Atmospheric Environment*, 41, 7377–7388. <https://doi.org/10.1016/j.atmosenv.2007.05.060>
- Bagnato, E., Oliveri, E., Acquavita, A., Covelli, S., Petranich, E., Barra, M., . . . Sprovieri, M. (2017). Hydrochemical mercury distribution and air-sea exchange over the submarine hydrothermal vents off-shore Panarea Island (Aeolian arc, Tyrrhenian Sea). *Marine Chemistry*, 194, 63–78. <https://doi.org/10.1016/j.marchem.2017.04.003>
- Bailey, J. C., & Rasmussen, M. H. (1997). Petrochemistry of Jurassic and Cretaceous tholeiites from Kong Karls Land, Svalbard, and their relation to Mesozoic magmatism in the Arctic. *Polar Research*, 16(1), 37–62.
- Barclay, R. S., McElwain, J. C., & Sageman, B. B. (2010). Carbon sequestration activated by a volcanic CO<sub>2</sub> pulse during Oceanic Anoxic Event 2. *Nature Geoscience*, 3, 205–208. <https://doi.org/10.1038/ngeo757>
- Batenburg, S. J., De Vleeschouwer, D., Sprovieri, M., Hilgen, F. J., Gale, A. S., Singer, B. S., . . . Montanari, A. (2016). Orbital control on the timing of oceanic anoxia in the Late Cretaceous. *Climate of the Past Discussion*, 12, 1995–2009. <https://doi.org/10.5194/cp-2015-182>
- Behar, F., Beaumont, V., & Penteado, H. D. B. (2001). Rock-Eval 6 technology: Performances and developments. *Oil & Gas Science and Technology*, 56(2), 111–134.
- Benoit, J. M., Gilmour, C. C., Mason, R. P., & Heyes, R. (1999). Sulfide controls on mercury speciation and bioavailability to methylating bacteria in sediment pore waters. *Environmental Science and Technology*, 33, 951–957. <https://doi.org/10.1021/es9808200>
- Benoit, J. M., Mason, R. P., Gilmour, C. C., & Aiken, G. R. (2001). Constants for mercury binding by dissolved organic matter isolates from the Florida Everglades. *Geochimica et Cosmochimica Acta*, 65, 4445–4451.
- Bin, C., Xiaoru, W., & Lee, F. S. C. (2001). Pyrolysis coupled with atomic absorption spectrometry for the determination of mercury in Chinese medical materials. *Analytica Chimica Acta*, 447, 161–169.
- Bird, P. (1998). Kinematic history of the Laramide orogeny in latitudes 35°–49°N, western United States. *Tectonics*, 17, 780–801.
- Blättler, C. L., Jenkyns, H. C., Reynard, L. M., & Henderson, G. M. (2011). Significant increases in global weathering during Oceanic Anoxic Events 1a and 2 indicated by calcium isotopes. *Earth and Planetary Science Letters*, 309, 77–88. <https://doi.org/10.1016/j.epsl.2011.06.029>
- Bottini, C., Cohen, A. S., Erba, E., Jenkyns, H. C., & Coe, A. L. (2012). Osmium isotope evidence for volcanism, weathering and ocean mixing during the early Aptian OAE 1a. *Geology*, 40, 583–586. <https://doi.org/10.1130/G33140.1>



- Bowman, K. L., Hammerschmidt, C. R., Lamborg, C. H., & Swarr, G. (2015). Mercury in the North Atlantic Ocean: The US GEOTRACES zonal and meridional sections. *Deep Sea Research Part II*, 116, 251–261. <https://doi.org/10.1016/j.dsr2.2014.07.004>
- Brown, P. E., Parsons, I., & Becker, S. M. (1987). Peralkaline volcanicity in the Arctic Basin—The Kap Washington Volcanics, petrology and palaeotectonics. *Journal of the Geological Society*, 144(5), 707–715.
- Brumsack, H. J. (2006). The trace metal content of recent organic carbon-rich sediments: Implications for Cretaceous black shale formation. *Palaeogeography, Palaeoclimatology, Palaeoecology*, 232, 344–361. <https://doi.org/10.1016/j.palaeo.2005.05.011>
- Bryan, S. E., & Ernst, R. E. (2008). Revised definition of Large Igneous Provinces (LIPs). *Earth Science Reviews*, 86, 175–202. <https://doi.org/10.1016/j.earscirev.2007.08.008>
- Buchan, K. L., & Ernst, R. E. (2006). The High Arctic Large Igneous Province (HALIP): Evidence for an associated giant radiating dyke swarm. *Large Igneous Provinces Commission*.
- Burchfiel, B. C., & Lipman, P. W. (1992). *The Cordilleran Orogen: Conterminous US* (No. 1). Boulder, CO: Geological Society of America.
- Burnett, J. A., Gallagher, L. T., & Hampton, M. J. (1998). Upper cretaceous. In P. R. Brown (Ed.), *Calcareous nannofossil biostratigraphy* (pp.132–199). Dordrecht, the Netherlands: Chapman-Hall.
- Charbonnier, G., & Föllmi, K. B. (2017). Mercury enrichments in lower Aptian sediments support the link between Ontong Java large igneous province activity and oceanic anoxic episode 1a. *Geology*, 45, 63–66. <https://doi.org/10.1130/G38207.1>
- Charbonnier, G., Morales, C., Duchamp-Alphonse, S., Westermann, S., Adatte, T., & Föllmi, K. B. (2017). Mercury enrichment indicates volcanic triggering of Valanginian environmental change. *Scientific Reports*, 7, 40808. <https://doi.org/10.1038/srep40808>
- Coccioni, R., & Galeotti, S. (2003). The mid-Cenomanian event: Prelude to OAE 2. *Palaeogeography, Palaeoclimatology, Palaeoecology*, 190, 427–440. [https://doi.org/10.1016/S0031-0182\(02\)00617-X](https://doi.org/10.1016/S0031-0182(02)00617-X)
- Coccioni, R., Sideri, M., Frontalini, F., & Montanari, A. (2016). The Rotalipor cushmani extinction at Gubbio (Italy): Planktonic foraminiferal testimony of the onset of the Caribbean large igneous province emplacement? In M. Menichetti, R. Coccioni, & A. Montanari (Eds.), *The stratigraphic record of Gubbio: Integrated stratigraphy of the late cretaceous-paleogene Umbria-Marche Pelagic Basin*, Geological Society of America Special Paper (Vol. 524, pp. 79–96). Boulder, CO: The Geological Society of America. [https://doi.org/10.1130/2016.2524\(06\)](https://doi.org/10.1130/2016.2524(06))
- Coffin, M. F., & Eldholm, O. (1994). Large igneous provinces: Crustal structure, dimensions, and external consequences. *Reviews of Geophysics*, 32, 1–36.
- Corfu, F., Polteau, S., Planke, S., Faleide, J. I., Svendsen, H., Zayonchek, A., & Stolbov, N. (2013). U–Pb geochronology of Cretaceous magmatism on Svalbard and Franz Josef Land, Barents Sea Large Igneous Province. *Geological Magazine*, 150(6), 1127–1135. <https://doi.org/10.1017/S0016756813000162>
- Courtillot, V., & Renne, P. R. (2003). On the ages of flood basalt events. *Comptes Rendus Géoscience*, 335, 113–140. [https://doi.org/10.1016/S1631-0713\(03\)00006-3](https://doi.org/10.1016/S1631-0713(03)00006-3)
- Davis, W. J., Schroder-Adams, C. J., Galloway, J. M., Herrle, J. O., & Pugh, A. T. (2017). U–Pb geochronology of bentonites from the Upper Cretaceous Kanguk Formation, Sverdrup Basin, Arctic Canada: Constraints on sedimentation rates, biostratigraphic correlations and the late magmatic history of the High Arctic Large Igneous Province. *Geological Magazine*, 154(4), 757–776.
- Demaison, G. J., & Moore, G. T. (1980). Anoxic environments and oil source bed genesis. *Organic Geochemistry*, 2, 9–31.
- Denne, R. A., Hinote, R. E., Breyer, J. A., Kosanke, T. H., Lees, J. A., Engelhardt-Moore, N., . . . Tur, N. (2014). The Cenomanian-Turonian Eagle Ford Group of South Texas: Insights on timing and paleoceanographic conditions from geochemistry and micropaleontologic analyses. *Palaeogeography, Palaeoclimatology, Palaeoecology*, 413, 2–28. <http://doi.org/10.1016/j.palaeo.2014.05.029>
- Desmarest, D., Grosheny, D., Beaudoin, B., Gardin, S., & Gauthier-Lafaye, F. (2007). High resolution stratigraphic record constrained by volcanic ash beds at the Cenomanian-Turonian boundary in the Western Interior Basin, USA. *Cretaceous Research*, 28, 561–582. <https://doi.org/10.1016/j.cretres.2006.08.009>
- Dickson, A. J., Gill, B. C., Ruhl, M., Jenkyns, H. C., Porcelli, D., Idiz, E., . . . Boorn, S.H. (2017). Molybdenum–isotope chemostratigraphy and paleoceanography of the Toarcian Oceanic Anoxic Event (Early Jurassic). *Paleoceanography*, 32, 813–829. <https://doi.org/doi:10.1002/2016PA003048>
- Dickson, A. J., Jenkyns, H. C., Porcelli, D., van den Boorn, S., & Idiz, E. (2016). Basin-scale controls on the molybdenum–isotope composition of seawater during Oceanic Anoxic Event 2 (Late Cretaceous). *Geochimica et Cosmochimica Acta*, 178, 291–306.
- Dickinson, W. R., & Lawton, T. F. (2001). Carboniferous to Cretaceous assembly and fragmentation of Mexico. *Geological Society of America Bulletin*, 113, 1142–1160.
- Du Vivier, A. D. C., Selby, D., Sageman, B. B., Jarvis, I., Gröcke, D. R., & Voigt, S. (2014). Marine  $^{187}\text{Os}/^{188}\text{Os}$  isotope stratigraphy reveals the interaction of volcanism and ocean circulation during Oceanic Anoxic Event 2. *Earth and Planetary Science Letters*, 389, 23–33. <https://doi.org/10.1016/j.epsl.2013.12.024>
- Du Vivier, A., Selby, D., Condon, D. J., Takashima, R., & Nishi, H. (2015). Pacific  $^{187}\text{Os}/^{188}\text{Os}$  isotopic chemistry and U–Pb geochronology: Synchronicity of global Os isotope change across OAE 2. *Earth and Planetary Science Letters*, 428, 204–216. <https://doi.org/10.1016/j.epsl.2015.07.020>
- Elderbak, K., & Leckie, M. R. (2016). Paleocirculation and foraminiferal assemblages of the Cenomanian-Turonian Bridge Creek Limestone bedding couplets: Productivity vs. dilution during OAE2. *Cretaceous Research*, 60, 52–77. <https://doi.org/10.1016/j.cretres.2015.11.009>
- Eldrett, J. S., Minisini, D., & Bergman, S. C. (2014). Decoupling of the carbon cycle during Oceanic Anoxic Event 2. *Geology*, 42, 567–570. <https://doi.org/10.1130/G35520.1>
- Eldrett, J. S., Ma, C., Bergman, S. C., Lutz, B., Gregory, F. J., Dodsworth, P., . . . Kelly, A. (2015a). An astronomically calibrated stratigraphic of the Cenomanian, Turonian and earliest Coniacian from the Cretaceous Western Interior Seaway, USA: Implications for global chronostratigraphy. *Cretaceous Research*, 56, 316–344. <https://doi.org/10.1016/j.cretres.2015.04.010>
- Eldrett, J. S., Ma, C., Bergman, S. C., Ozkan, A., Minisini, D., Lutz, B., . . . Kelly, S. J. (2015b). Origin of limestone-marlstone cycles: Astronomical forcing of organic rich sedimentary rocks from the Cenomanian to early Coniacian of the Cretaceous Western Interior Seaway, USA. *Earth and Planetary Science Letters*, 423, 98–113. <https://doi.org/10.1016/j.epsl.2015.04.026>
- Eldrett, J. S., Dodsworth, P., Bergman, S. C., Wright, M., & Minisini, D. (2017). Water-mass evolution in the Cretaceous Western Interior Seaway of North America and Equatorial Atlantic. *Climate of the Past*, 13(7), 855–878. <https://doi.org/10.5194/cp-13-855-2017>
- Erba, E. (1994). Nannofossils and superplumes: The early Aptian “nannoconid crisis”. *Paleoceanography*, 9, 483–501. <https://doi.org/10.1029/94PA00258>
- Erba, E. (2004). Calcareous nannofossils and Mesozoic oceanic anoxic events. *Marine Micropaleontology*, 52(1), 85–106.
- Erba, E., Duncan, R. A., Bottini, C., Tiraboschi, D., Weissert, H., Jenkyns, H. C., & Malinverno, A. (2015). Environmental consequences of Ontong Java Plateau and Keruelen Plateau volcanism. In C. R. Neal et al. (Eds.), *The origin, evolution, and environmental consequences of oceanic large igneous provinces*, Geological Society of America Special Paper (Vol. 511, pp. 271–303). Boulder, CO: The Geological Society of America. <https://doi.org/10.3301/ROL.2015.131>

- Erbacher, J., Friedrich, O., Wilson, P. A., Birch, H., & Mutterlose, J. (2005). Stable organic carbon isotope stratigraphy across Oceanic Anoxic Event 2 of Demerara Rise, western tropical Atlantic. *Geochemistry, Geophysics, Geosystems*, 6, Q06010. <https://doi.org/10.1029/2004GC000850>
- Erbacher, J., Huber, B. T., Norris, R. D., & Markey, M. (2001). Increased thermohaline stratification as a possible cause for an ocean anoxic event in the Cretaceous period. *Nature*, 409, 325–327. <https://doi.org/10.1038/35053041>
- Estrada, S. (2015). Geochemical and Sr-Nd isotope variations within Cretaceous continental flood-basalt suites of the Canadian High Arctic, with a focus on the Hassel Formation basalts of northeast Ellesmere Island. *International Journal of Earth Sciences/Geologische Rundschau*, 104, 1981–2005. <https://doi.org/10.1007/s00531-014-1066-x>
- Estrada, S., & Henjes-Kunst, F. (2004). Volcanism in the Canadian High Arctic related to the opening of the Arctic Ocean. *Zeitschrift Der Deutschen Geologischen Gesellschaft*, 154(4), 579–603.
- Evenchick, C. A., Davis, W. J., Bédard, J. H., Hayward, N., & Friedman, R. M. (2015). Evidence for protracted High Arctic Large Igneous Province magmatism in the central Sverdrup Basin from stratigraphy, geochronology, and paleodepths of saucer-shaped sills. *Geological Society of America Bulletin*, 127(9–10), 1366–1390. <https://doi.org/10.1130/B31190.1>
- Falzone, F., Petrizzo, M. R., Jenkyns, H. C., Gale, A. S., & Tsikos, H. (2016). Planktonic foraminiferal biostratigraphy and assemblage composition across the Cenomanian-Turonian boundary interval at Clot Chevalier (Vocontian Basin, SE France). *Cretaceous Research*, 59, 69–97. <https://doi.org/10.1016/j.cretres.2015.10.028>
- Forster, A., Schouten, S., Moriya, K., Wilson, P. A., & Sinninghe Damsté, J. S. (2007). Tropical warming and intermittent cooling during the Cenomanian/Turonian oceanic anoxic event 2: Sea surface temperature records from the equatorial Atlantic. *Paleoceanography*, 22, PA1219. <https://doi.org/10.1029/2006PA001349>
- Friedrich, O., Erbacher, J., & Mutterlose, J. (2006). Paleoenvironmental changes across the Cenomanian/Turonian Boundary Event (Oceanic Anoxic Event 2) as indicated by benthic foraminifera from the Demerara Rise (ODP Leg 207). *Revue de Micropaléontologie*, 49, 121–139. <https://doi.org/10.1016/j.revmic.2006.04.003>
- Friedrich, O., Erbacher, J., Wilson, P. A., Moriya, K., & Mutterlose, J. (2009). Paleoenvironmental changes across the Mid Cenomanian Event in the tropical Atlantic Ocean (Demerara Rise, ODP Leg 207) inferred from benthic foraminifera assemblages. *Marine Micropaleontology*, 71, 28–40. <https://doi.org/10.1016/j.marmicro.2009.01.002>
- Gale, A. S., & Christensen, W. K. (1996). Occurrence of the belemnite *Actinocamax plenus* in the Cenomanian of SE France and its significance. *Bulletin of the Geological Society of Denmark*, 43, 68–77.
- Gambacorta, G., Jenkyns, H. C., Russo, F., Tsikos, H., Wilson, P. A., Faucher, G., & Erba, E. (2015). Carbon- and oxygen-isotope records of mid-Cretaceous Tethyan pelagic sequences from the Umbria-Marche and Belluno Basins (Italy). *Newsletters on Stratigraphy*, 48, 299–323. <https://doi.org/10.1127/nos/2015/0066>
- Gehrke, G. E., Blum, J. D., & Meyers, P. A. (2009). The geochemical behaviour and isotopic composition of Hg in a mid-Pleistocene western Mediterranean sapropel. *Geochimica et Cosmochimica Acta*, 73, 1651–1665. <http://doi.org/10.1016/j.gca.2008.12.012>
- Gong, Q., Wang, X., Zhao, L., Grasby, S. E., Chen, Z. Q., Zhang, L., . . . Li, Z. (2017). Mercury spikes suggest volcanic driver of the Ordovician-Silurian mass extinction. *Scientific Reports*, 7, 5304. <http://doi.org/10.1038/s41598-017-05524-5>
- Grasby, S. E., Sanei, H., Beauchamp, B., & Chen, Z. (2013). Mercury deposition through the Permo-Triassic Biotic Crisis. *Chemical Geology*, 351, 209–216. <https://doi.org/10.1016/j.chemgeo.2013.05.022>
- Hardas, P., & Mutterlose, J. (2006). Calcareous nannofossil biostratigraphy of the Cenomanian/Turonian boundary interval of ODP Leg 207 at the Demerara Rise. *Revue De Micropaléontologie*, 49, 165–179.
- Hardenbol, J. A. N., Thierry, J., Farley, M. B., Jacquin, T., Graciansky, P. C. D., & Vail, P. R. (1998). Mesozoic and Cenozoic sequence chronostratigraphic framework of European basins. *Special Publication SEPM Society for Sedimentary Geology*, 60. <https://doi.org/10.2110/sepm.105>
- Hay, W. W. (2009). Cretaceous oceans and ocean modeling. *Special Publication SEPM Society for Sedimentary Geology*, 91, 243–271.
- Hetzl, A., Böttcher, M. E., Wortmann, U. G., & Brumsack, H. J. (2009). Paleo-redox conditions during OAE 2 reflected in Demerara Rise sediment geochemistry (ODP Leg 207). *Palaeogeography, Palaeoclimatology, Palaeoecology*, 273, 302–328. <https://doi.org/10.1016/j.palaeo.2008.11.005>
- Hinkley, T. K., Lamothe, P. J., Wilson, S. A., Finnegan, D. L., & Gerlach, T. M. (1999). Metal emissions from Kilauea, and a suggested revision of the estimated worldwide metal output by quiescent degassing of volcanoes. *Earth and Planetary Science Letters*, 170, 315–325. [https://doi.org/10.1016/S0012-821X\(99\)00103-X](https://doi.org/10.1016/S0012-821X(99)00103-X)
- Holmden, C., Jacobson, A. D., Sageman, B. B., & Hurtgen, M. T. (2016). Response of the Cr isotope proxy to Cretaceous Oceanic Anoxic Event 2 in a pelagic carbonate succession from the Western Interior Seaway. *Geochimica et Cosmochimica Acta*, 186, 277–295. <https://doi.org/10.1016/j.gca.2016.04.039>
- Jaenicke, R. (1980). Atmospheric aerosols and global climate. *Journal of Aerosol Sciences*, 11, 577–588. [https://doi.org/10.1016/0021-8502\(80\)90131-7](https://doi.org/10.1016/0021-8502(80)90131-7)
- Jarvis, I., Carson, G. A., Cooper, M. K. E., Hart, M. B., Leary, P. N., Tocher, B. A., . . . Rosenfeld, A. (1988). Microfossil assemblages and the Cenomanian-Turonian (late Cretaceous) oceanic anoxic event. *Cretaceous Research*, 9, 3–103. [https://doi.org/10.1016/0195-6671\(88\)90003-1](https://doi.org/10.1016/0195-6671(88)90003-1)
- Jarvis, I., Gale, A. S., Jenkyns, H. C., & Pearce, M. A. (2006). Secular variation in Late Cretaceous carbon isotopes: A new  $\delta^{13}\text{C}$  carbonate reference curve for the Cenomanian-Campanian (99.6–70.6 Ma). *Geological Magazine*, 143, 561–608. <https://doi.org/10.1017/S0016756806002421>
- Jarvis, I., Lignum, J. S., Gröcke, D. R., Jenkyns, H. C., & Pearce, M. A. (2011). Black Shale deposition, atmospheric CO<sub>2</sub> drawdown, and cooling during the Cenomanian-Turonian Oceanic Anoxic Event. *Paleoceanography*, 26, PA3201. <http://doi.org/10.1029/2010PA002081>
- Jenkyns, H. C. (1980). Cretaceous anoxic events: From continents to oceans. *Journal of Geological Society*, 137, 171–188. <https://doi.org/10.1144/gsjgs.137.2.0171>
- Jenkyns, H. C. (1988). The early Toarcian (Jurassic) anoxic event: Stratigraphic, sedimentary, and geochemical evidence. *American Journal of Science*, 288, 101–151.
- Jenkyns, H. C. (2010). Geochemistry of oceanic anoxic events. *Geochemistry Geophysics Geosystems*, 11, Q03004. <https://doi.org/10.1029/2009GC002788>
- Jenkyns, H. C., Dickson, A. J., Ruhl, M., & Van Den Boorn, S. H. J. M. (2017). Basalt-seawater interaction, the Plenius Cold Event, enhanced weathering and geochemical change: Deconstructing Oceanic Anoxic Event 2 (Cenomanian-Turonian, Late Cretaceous). *Sedimentology*, 64, 16–43. <https://doi.org/10.1111/sed.12305>
- Jiménez-Berrocó, A., MacLeod, K. G., Martin, E. E., Bourbon, E., Londono, C. I., & Basak, C. (2010). Nutrient trap for Late Cretaceous organic-rich black shales in the tropical North Atlantic. *Geology*, 38, 1111–1114. <https://doi.org/10.1130/G31195.1>
- Jones, C. E., & Jenkyns, H. C. (2001). Seawater strontium isotopes, oceanic anoxic events, and seafloor hydrothermal activity in the Jurassic and Cretaceous. *American Journal of Science*, 301, 112–149. <https://doi.org/10.2475/ajs.301.2.112>

- Jones, D. S., Martini, A. M., Fike, D. A., & Kaiho, K. (2017). A volcanic trigger for the Late Ordovician mass extinction? Mercury data from south China and Laurentia. *Geology*, 45(7), 631–634.
- Joo, Y. J., & Sageman, B. B. (2014). Cenomanian to Campanian carbon isotope chemostratigraphy from the Western Interior Basin, USA. *Journal of Sedimentary Research*, 84, 529–542. <https://doi.org/10.2110/jsr.2014.38>
- Kump, L. R., & Slingerland, R. L. (1999). Circulation and stratification of the early Turonian Western Interior Seaway: Sensitivity to a variety of forcings. In E. Barrera & C. Johnson (Eds.), *Evolution of cretaceous ocean-climate system, Geological Society of America Special Paper* (Vol. 332, pp. 181–190). Boulder, CO: The Geological Society of America.
- Kuroda, J., Ogawa, N. O., Tanimizu, M., Coffin, M. F., Tokuyama, H., Kitazato, H., & Ohkouchi, N. (2007). Contemporaneous massive subaerial volcanism and Late Cretaceous oceanic anoxic event 2. *Earth and Planetary Science Letters*, 256, 211–223. <https://doi.org/10.1016/j.epsl.2007.01.027>
- Kuroda, J., Tanimizu, M., Hori, R. S., Suzuki, K., Ogawa, N. O., Tejada, M. L. G., . . . Ohkouchi, N. (2011). Lead isotopic record of Barremian–Aptian marine sediments: Implications for large igneous provinces and the Aptian climatic crisis. *Earth and Planetary Science Letters*, 307, 126–134. <https://doi.org/10.1016/j.epsl.2011.04.021>
- Kuypers, M. M. M., Pancost, R. D., & Sinninghe Damste, J. S. (1999). A large and abrupt fall in atmospheric CO concentration 2 during Cretaceous times. *Nature*, 399, 342–345. <https://doi.org/10.1038/20659>
- Lamolda, M. A., Gorostidi, A., & Paul, C. R. C. (1994). Quantitative estimates of calcareous nannofossil changes across the Plenus Marls (latest Cenomanian), Dover, England: Implications for the generation of the Cenomanian–Turonian Boundary Event. *Cretaceous Research*, 15, 143–164. <https://doi.org/10.1006/cres.1994.1007>
- Larson, R. L., & Erba, E. (1999). Onset of the mid-Cretaceous greenhouse in the Barremian–Aptian: Igneous events and the biological, sedimentary and geochemical responses. *Paleoceanography*, 14, 663–678. <https://doi.org/10.1029/1999PA900040>
- Lindqvist, O., & Rodhe, H. (1985). Atmospheric mercury—A review. *Tellus, Series B*, 37, 136–159. <https://doi.org/10.1111/j.1600-0889.1985.tb00062.x>
- Liu, X., Xu, L., Chen, Q., Sun, L., Wand, Y., Yan, H., . . . Huang, J. (2012). Historical change of mercury pollution in remote Yongle archipelago, South China Sea. *Chemosphere*, 87, 549–556. <https://doi.org/10.1016/j.chemosphere.2011.12.065>
- Lowery, C. M., Corbett, M. J., Leckie, M., Watkins, D., Romero, A. M., & Pramudito, A. (2014). Foraminifers and nannofossil paleoecology and paleoceanography of the Cenomanian–Turonian Eagle Ford Shale of southern Texas. *Palaeogeography, Palaeoclimatology, Palaeoecology*, 413, 49–65. <https://doi.org/10.1016/j.palaeo.2014.07.025>
- Luzieux, L. D. A., Heller, F., Spikings, R., Vallejo, C. F., & Winkler, W. (2006). Origin and Cretaceous tectonic history of the coastal Ecuadorian forearc between 1°N and 3°S: Paleomagnetic, radiometric and fossil evidence. *Earth and Planetary Science Letters*, 249(3), 400–414.
- Ma, C., Meyers, S. R., Sageman, B. B., Singer, B. S., & Jicha, B. R. (2014). Testing the astronomical time scale for Oceanic Anoxic Event 2, and its extension into Cenomanian Strata of the Western Interior Basin (U.S.A.). *Geological Society of America Bulletin*, 126, 974–989. <https://doi.org/10.1130/B30922.1>
- MacLeod, K. G., Martin, E. E., & Blair, S. W. (2008). Nd isotopic excursion across Cretaceous oceanic anoxic event 2 (Cenomanian–Turonian) in the tropical North Atlantic. *Geology*, 36, 811–814. <https://doi.org/10.1130/G24999A.1>
- Maher, H. D. Jr., (2001). Manifestations of Cretaceous High Arctic large igneous province in Svalbard. *Journal of Geology*, 109, 91–104. <https://doi.org/10.1086/317960>
- Mahoney, J., Nicollet, C., & Dupuy, C. (1991). Madagascar basalts: Tracking oceanic and continental sources. *Earth and Planetary Science Letters*, 104(2–4), 350–363.
- Mahoney, J. J., Storey, M., Duncan, R. A., Spencer, K. J., & Pringle, M. (1993). Geochemistry and age of the Ontong Java Plateau. In M. S. Pringle et al. (Eds.), *The mesozoic Pacific: Geology, tectonics, and volcanism* (Vol. 77, pp. 233–261). Washington, DC: American Geophysical Union. <https://doi.org/10.1029/GM077p0233>
- Martin, E. E., MacLeod, K. G., Jimenez-Berrococo, A., & Bourbon, E. (2012). Water mass circulation on Demerara Rise during the Late Cretaceous based on Nd isotopes. *Earth and Planetary Science Letters*, 327/328, 111–120. <https://doi.org/10.1016/j.epsl.2012.01.037>
- Mason, R. P., Choi, A. L., Fitzgerald, W. F., Hammerschmidt, C. R., Lamborg, C. H., Soerensen, A. L., & Sunderland, E. M. (2012). Mercury biogeochemical cycling in the ocean and policy implications. *Environmental Research*, 119, 101–117. <https://doi.org/10.1016/j.envres.2012.03.013>
- Mather, T. A., Pyle, D. M., & Oppenheimer, C. (2003). Tropospheric volcanic aerosol. In A. Robock & C. Oppenheimer (Eds.), *Volcanism and the Earth's Atmosphere, Geophysical Monograph Series* (Vol. 139, pp. 189–212). Washington, DC: American Geophysical Union. <https://doi.org/10.1029/139GM12>
- Méhay, S., Keller, C. E., Bernasconi, S. M., Weissert, H., Erba, E., Bottini, C., & Hochuli, P. A. (2009). A volcanic CO<sub>2</sub> pulse triggered the Cretaceous oceanic anoxic event 1a and a biocalcification crisis. *Geology*, 37, 819–822. <https://doi.org/10.1130/G30100A.1>
- Meyers, P. A., Bernasconi, S., & Forster, M. A. (2006). Origin and accumulation of organic matter in expanded Albian to Santonian black shale sequences on the Demerara Rise, South American margin. *Organic Geochemistry*, 37, 1816–1830. <https://doi.org/10.1016/j.orggeochem.2006.08.009>
- Meyers, S. R. (2007). Production and preservation of organic matter: The significance of iron. *Paleoceanography*, 22, PA4211. <https://doi.org/10.1029/2006PA001332>
- Minisini, D., Eldrett, J., Bergman, S. C., & Forkner, R. (2017). Chronostratigraphic framework and depositional environments in the organic-rich, mudstone-dominated Eagle Ford Group, Texas, USA. *Sedimentology*. <https://doi.org/10.1111/sed.12437>, in press.
- Mitchell, S. F., & Carr, I. T. (1998). Foraminifers response to mid-Cenomanian (Upper Cretaceous) palaeoceanographic events in the Anglo-Paris Basin (Northwest Europe). *Palaeogeography, Palaeoclimatology, Palaeoecology*, 137, 103–125. [https://doi.org/10.1016/S0031-0182\(97\)00087-4](https://doi.org/10.1016/S0031-0182(97)00087-4)
- Musavv-Moussavou, B., Danelian, T., Baudin, F., Coccioni, R., & Fröhlich, F. (2007). The radiolarian biotic response during OAE2. A high-resolution study across the Bonarelli level at Bottaccione (Gubbio, Italy). *Revue De Micropaléontology*, 50, 253–287. <https://doi.org/10.1016/j.revmic.2007.07.002>
- Neal, C. R., Mahoney, J. J., Kroenke, L. W., Duncan, R. A., & Pettersen, M. G. (1997). The Ontong Java plateau. In J. J. Mahoney & M. F. Coffin (Eds.), *Large igneous provinces: Continental, oceanic, and planetary flood volcanism, Geophysical Monograph Series* (Vol. 100, pp. 183–216). Washington, DC: American Geophysical Union. <https://doi.org/10.1029/GM100p018>
- Niessen, S., Foucher, D., Clarisse, O., Fischer, J. C., Mikac, N., Kwokal, Z., . . . Horvat, M. (2003). Influence of sulphur cycle on mercury methylation in estuarine sediment (Seine estuary, France). *Journal de Physique IV*, 107, 953–956. <http://doi.org/10.1051/jp:20030456>
- Orth, C. J., Attrep, M., Quintana, L. R., Elder, W. P., Kauffman, E. G., Diner, R., & Villamil, T. (1993). Elemental abundance anomalies in the late Cenomanian extinction interval: A search for the source(s). *Earth and Planetary Science Letters*, 117(1–2), 189–204.
- Outridge, P. M., Sanei, H., Stern, G. A., Hamilton, P. B., & Goodarzi, F. (2007). Evidence for control of mercury accumulation rates in Canadian High Arctic lake sediments by variations of aquatic primary productivity. *Environment Science and Technology*, 41, 5259–5265. <https://doi.org/10.1021/es070408x>

- Owens, J. D., Lyons, T. W., Hardisty, D. S., Lowery, C. M., Lu, Z., Lee, B., & Jenkyns, H. C. (2017). Patterns of local and global redox variability during the Cenomanian-Turonian Boundary Event (Oceanic Anoxic Event 2) recorded in carbonates and shales from central Italy. *Sedimentology*, 64, 168–185. <https://doi.org/10.1111/sed.12352>
- Paul, C. R. C., Mitchell, S. F., Marshall, J. D., Leafy, P. N., Gale, A. S., Duane, A. M., & Ditchfield, P. W. (1994). Palaeoceanographic events in the Middle Cenomanian of Northwest Europe. *Cretaceous Research*, 15, 707–738. <https://doi.org/10.1006/cres.1994.1039>
- Pegram, W. J., & Turekian, K. K. (1999). The osmium isotopic composition change of Cenozoic sea water as inferred from a deep-sea core corrected for meteoritic contributions. *Geochimica et Cosmochimica Acta*, 63, 4053–4058. [https://doi.org/10.1016/S0016-7037\(99\)00308-7](https://doi.org/10.1016/S0016-7037(99)00308-7)
- Percival, L. M. E., Cohen, A. S., Davies, M. K., Dickson, A. J., Hesselbo, S. P., Jenkyns, H. C., ... Xu, W. (2016). Osmium isotope evidence for two pulses of increased continental weathering linked to Early Jurassic volcanism and climate change. *Geology*, 44(9), 759–762.
- Percival, L. M. E., Ruhl, M., Hesselbo, S. P., Jenkyns, H. C., Mather, T. A., & Whiteside, J. H. (2017). Mercury evidence for pulsed volcanism during the end-Triassic mass extinction. *Proceedings of the National Academy of Sciences United States of America*, 114(30), 7929–7934.
- Percival, L. M. E., Witt, M. L. I., Mather, T. A., Hermoso, M., Jenkyns, H. C., Hesselbo, S. P., ... & Ruhl, M. (2015). Globally enhanced mercury deposition during the end-Plenian extinction and Toarcian OAE: A link to the Karoo-Ferrar large igneous province. *Earth and Planetary Science Letters*, 428, 267–280. <https://doi.org/10.1016/j.epsl.2015.06.064>
- Pessagno, E. A. (1969). Upper Cretaceous stratigraphy of the western Gulf Coast area of Mexico, Texas and Arkansas. *Geological Society of America Memoirs*, 111, 1–139. <https://doi.org/10.1130/MEM111-p1>
- Pogge von Strandmann, P. A. E., Jenkyns, H. C., & Woodfine, R. G. (2013). Lithium isotope evidence for enhanced weathering during Oceanic Anoxic Event 2. *Nature Geoscience*, 6, 668–672. <https://doi.org/10.1016/j.epsl.2015.09.052>
- Pyle, D. M., & Mather, T. A. (2003). The importance of volcanic emissions for the global atmospheric mercury cycle. *Atmospheric Environment*, 37, 5115–5124. <https://doi.org/10.1016/j.atmosenv.2003.07.011>
- Polteau, S., Hendriks, B. W. H., Planke, S., Ganerød, M., Corfu, F., Faleide, J. I., ... Myklebust, R. (2015). The Early Cretaceous Barents Sea Sill Complex: Distribution,  $^{40}\text{Ar}/^{39}\text{Ar}$  geochronology, and implications for carbon gas formation. *Palaeogeography, Palaeoclimatology, Palaeoecology*, 441, 83–95. <https://doi.org/10.1016/j.palaeo.2015.07.007>
- Rampino, M. R., & Strothers, R. B. (1988). Flood basalt volcanism during the past 250 million years. *Science*, 241, 663–668.
- Roth, P. H. (1978). Cretaceous nannoplankton biostratigraphy and oceanography of the northwestern Atlantic Ocean. *Initial Reports of the Deep Sea Drilling Project*, 44, 731–759.
- Ruiz, W. L. G., & Tomiyasu, T. (2015). Distribution of mercury in sediments from Kagoshima Bay, Japan, and its relationship with physical and chemical factors. *Environmental Earth Sciences*, 74, 1175–1188. <https://doi.org/10.1007/s12665-015-4104-5>
- Sageman, B. B., Meyers, S. R., & Arthur, M. A. (2006). Orbital timescale for the Cenomanian-Turonian boundary stratotype and OAE II, central Colorado, USA. *Geology*, 34, 125–128. <https://doi.org/10.1130/G22074.1>
- Sanei, H., Grasby, S., & Beauchamp, B. (2012). Latest Permian mercury anomalies. *Geology*, 40, 63–66. <https://doi.org/10.1130/G32596.1>
- Schlanger, S. O., Arthur, M. A., Jenkyns, H. C., & Scholte, P. A. (1987). The Cenomanian-Turonian Oceanic Anoxic Event, I. Stratigraphy and distribution of organic carbon-rich beds and the marine  $\delta^{13}\text{C}$  excursion. In J. Brooks & A. J. Fleet (Eds.), *Marine petroleum source rocks*, Geological Society Special Publication (Vol. 26, pp. 371–399). Oxford, UK: Blackwell. <https://doi.org/10.1144/GSL.SP.1987.026.01.24>
- Schlanger, S. O., & Jenkyns, H. C. (1976). Cretaceous anoxic events: Causes and consequences. *Geologie en Mijnbouw*, 55, 179–184.
- Schroeder, W. H., & Munthe, J. (1998). Atmospheric mercury—An overview. *Atmospheric Environment*, 32, 809–822. [https://doi.org/10.1016/S1352-2310\(97\)00293-8](https://doi.org/10.1016/S1352-2310(97)00293-8)
- Shipboard Scientific Party (2004a). Site 1258. In J. Erbacher et al. (Eds.), *Proceedings of the ocean drilling program initial reports* (Vol. 207, pp. 1–117). College Station, TX: Ocean Drilling Program. <https://doi.org/10.2973/odp.proc.ir.207.104.2004>
- Shipboard Scientific Party (2004b). Site 1260. In J. Erbacher, D. C. Mosher, & M. J. Malone (Eds.), *Proceedings of the Ocean Drilling Program Initial Reports* (Vol. 207, pp. 1–35). College Station, TX: Ocean Drilling Program. <https://doi.org/10.2973/odp.proc.ir.207.107.2004>
- Sial, A. N., Chen, J., Lacerda, L. D., Frei, R., Tewari, V. C., Pandit, M. K., ... Korte, C. (2016). Mercury enrichment and Hg isotopes in Cretaceous-Paleogene boundary successions: Links to volcanism and palaeoenvironmental impacts. *Cretaceous Research*, 66, 60–81. <https://doi.org/10.1016/j.cretres.2016.05.006>
- Sial, A. N., Chen, J., Lacerda, L. D., Peralta, S., Gaucher, C., Frei, R., & Pereira, N. S. (2014). High-resolution Hg chemostratigraphy: A contribution to the distinction of chemical fingerprints of the Deccan volcanism and Cretaceous-Paleogene Boundary impact event. *Palaeogeography, Palaeoclimatology, Palaeoecology*, 414, 98–115. <https://doi.org/10.1016/j.palaeo.2014.08.013>
- Sial, A. N., Lacerda, L. D., Ferreira, V. P., Frei, R., Marquillas, R. A., Barbosa, J. A., ... Pereira, N. S. (2013). Mercury as a proxy for volcanic activity during extreme environmental turnover: The Cretaceous–Paleogene transition. *Palaeogeography, Palaeoclimatology, Palaeoecology*, 387, 153–164. <https://doi.org/10.1016/j.palaeo.2013.07.019>
- Sinninghe Damsté, J. S., & Köster, J. (1998). A euxinic southern North Atlantic Ocean during the Cenomanian-Turonian oceanic anoxic event. *Earth and Planetary Science Letters*, 158, 165–173. [https://doi.org/10.1016/S0012-821X\(98\)00052-1](https://doi.org/10.1016/S0012-821X(98)00052-1)
- Sinninghe Damsté, J. S., van Bentum, E. C., Reichert, G. J., Pross, J., & Schouten, S. (2010). A CO<sub>2</sub> decrease-driven cooling and increased latitudinal temperature gradient during the mid-Cretaceous Oceanic Anoxic Event 2. *Earth and Planetary Science Letters*, 293, 97–103. <https://doi.org/10.1016/j.epsl.2010.02.027>
- Slingerland, R., Kump, L. R., Arthur, M. A., Fawcett, P. J., Sageman, B. B., & Barron, E. J. (1996). Estuarine circulation in the Turonian Western Interior seaway of North America. *Geological Society of America Bulletin*, 108, 941–952. [https://doi.org/10.1130/0016-7606\(1996\)108<0941:ECITW>2.3.CO;2](https://doi.org/10.1130/0016-7606(1996)108<0941:ECITW>2.3.CO;2)
- Snow, L. J., Duncan, R. A., & Bralower, T. J. (2005). Trace element abundances in the Rock Canyon Anticline, Pueblo, Colorado, marine sedimentary section and their relationship to Caribbean plateau construction and oxygen anoxic event 2. *Paleoceanography*, 20, PA3005. <https://doi.org/10.1029/2004PA001093>
- Spikings, R., Cochrane, R., Villagomez, D., Van der Lelij, R., Vallejo, C., Winkler, W., & Beate, B. (2015). The geological history of northwestern South America: From Pangaea to the early collision of the Caribbean large igneous province (290–75Ma). *Gondwana Research*, 27(1), 95–139. <https://doi.org/10.1016/j.gr.2014.06.004>
- Storey, M., Mahoney, J. J., Saunders, A. D., Duncan, R. A., Kelley, S. P., & Coffin, M. F. (1995). Timing of hot spot-related volcanism and the breakup of Madagascar and India. *Science*, 267, 852–855.
- Tarduno, J. A., Brinkman, D. B., Renne, P. R., Cottrell, R. D., Scher, H., & Castillo, P. (1998). Evidence for extreme climatic warmth from Late Cretaceous Arctic vertebrates. *Science*, 282(5397), 2241–2243.
- Tarduno, J. A., Sliter, W. V., Kroenke, L., Leckie, M., Mayer, H., Mahoney, J. J., ... Winterer, E. L. (1991). Rapid formation of Ontong Java Plateau by Aptian mantle plume volcanism. *Science*, 254, 399–403. <https://doi.org/10.1126/science.254.5030.399>
- Taylor, B. (2006). The single largest oceanic plateau: Ontong Java-Manihiki-Hikurangi. *Earth and Planetary Science and Letters*, 241(3), 372–380. <https://doi.org/10.1016/j.epsl.2005.11.049>



- Tegner, C., Storey, M., Holm, P. M., Thorarinsson, S. B., Zhao, X., Lo, C. H., & Knudsen, M. F. (2011). Magmatism and Eureka deformation in the High Arctic Large Igneous Province: 40Ar-39Ar age of Kap Washington Group volcanics, North Greenland. *Earth and Planetary Science and Letters*, 303, 203–214. <https://doi.org/10.1016/j.epsl.2010.12.047>
- Tejada, M. L. G., Mahoney, J. J., Castillo, P. R., Ingle, S. P., Sheth, H. C., & Weis, D. (2004). Pin-pricking the elephant: Evidence on the origin of the Ontong Java Plateau from Pb-Sr-Hf-Nd isotopic characteristics of ODP Leg 192 basalts. *Geological Society London Special Publications*, 229(1), 133–150.
- Tejada, M. L. G., Mahoney, J. J., Duncan, R. A., & Hawkins, M. P. (1996). Age and geochemistry of basement and alkalic rocks of Malaita and Santa Isabel, Solomon Islands, southern margin of Ontong Java Plateau. *Journal of Petrology*, 37(2), 361–394.
- Tejada, M. L. G., Mahoney, J. J., Neal, C. R., Duncan, R. A., & Pettersson, M. G. (2002). Basement geochemistry and geochronology of Central Malaita, Solomon Islands, with implications for the origin and evolution of the Ontong Java Plateau. *Journal of Petrology*, 43(3), 449–484.
- Tejada, M. L. G., Suzuki, K., Kuroda, J., Coccioni, R., Mahoney, J. J., Ohkouchi, N., . . . Tatsumi, Y. (2009). Ontong Java plateau eruption as a trigger for the early Aptian oceanic anoxic event. *Geology*, 37, 855–858. <https://doi.org/10.1130/G25763A.1>
- Thibodeau, A. M., Ritterbush, K., Yager, J. A., West, A. J., Ibarra, Y., Bottjer, D. J., . . . Corsetti, F. A. (2016). Mercury anomalies and the timing of biotic recovery following the end-Triassic mass extinction. *Nature Communication*, 7, 11147. <https://doi.org/10.1038/ncomms11147>
- Thordarson, T. (2004). Accretionary-lapilli-bearing pyroclastic rocks at ODP Leg Site 192 1184: A record of subaerial phreatomagmatic eruptions on the Ontong Java Plateau. In J. G. Fitton et al. (Eds.), *Origin and evolution of the Ontong Java Plateau, Geological Society Special Publication* (Vol. 229, pp. 275–306). <https://doi.org/10.1144/GSL.SP.2004.229.01.16>
- Torsvik, T. H., Tucker, R. D., Ashwal, L. D., Eide, E. A., Rakotosolof, N. A., & De Wit, M. J. (1998). Late Cretaceous magmatism in Madagascar: Palaeomagnetic evidence for a stationary Marion hotspot. *Earth and Planetary Science Letters*, 164(1), 221–232.
- Trabucho Alexandre, J., Tuentner, E., Henstra, G. A., van der Zwan, K. J., van de Wal, R. S. W., Dijkstra, H. A., & de Boer, P. L. (2010). The mid-Cretaceous North Atlantic nutrient trap: Black shales and OAEs. *Paleoceanography*, 25, PA4201. <https://doi.org/10.1029/2010PA001925>
- Tribouillard, N., Algeo, T., Lyons, T. W., & Riboulleau, A. (2006). Trace metals as paleoredox and paleoproductivity proxies: An update. *Chemical Geology*, 232, 12–32. <https://doi.org/10.1016/j.chemgeo.2006.02.012>
- Tribouillard, N., Ramdani, A., & Trentesaux, A. (2005). Controls on organic accumulation in Late Jurassic shales of northwestern Europe as inferred from trace-metal geochemistry. In N. Harris (Ed.), *The deposition of organic-carbon-rich sediments: Models, mechanisms, and consequences, Special Publication SEPM* (Vol. 82, pp. 145–164). <https://doi.org/10.2113/175.5.491>
- Tsikos, H., Jenkyns, H. C., Walsworth-Bell, B., Petrizzo, M. R., Forster, A., Kolonic, S., . . . Sinninghe Damsté, J. S. (2004). Carbon-isotope stratigraphy recorded by the Cenomanian-Turonian oceanic anoxic event: Correlation and implications based on three key localities. *Journal of the Geological Society*, 161, 711–719. <https://doi.org/10.1144/0016-764903-077>
- Turgeon, S. C., & Creaser, R. A. (2008). Cretaceous oceanic anoxic event 2 triggered by a massive magmatic episode. *Nature*, 454, 323–326. <https://doi.org/10.1038/nature07076>
- van Bentum, E. C., Hetzel, A., Brumsack, H. J., Forster, A., Reichart, G. J., & Sinninghe Damsté, J. S. (2009). Reconstruction of water column anoxia in the equatorial Atlantic during the Cenomanian-Turonian oceanic anoxic event using biomarker and trace metal proxies. *Paleoceanography, Palaeoclimatology, Palaeoecology*, 280, 489–498. <https://doi.org/10.1016/j.paleo.2009.07.003>
- van Helmond, N. A. G. M., Sluijs, A., Reichart, G. J., Sinninghe Damsté, J. S., & Slomp, C. P. (2013). A perturbed hydrological cycle during Oceanic Anoxic Event 2. *Geology*, 42, 123–126. <https://doi.org/10.1130/G34929.1>
- Van Helmond, N. A. G. M., Sluijs, A., Papadomanolaki, N. M., Plint, A. G., Gröcke, D. R., Pearce, M. A., . . . Brinkhuis, H. (2016). Equatorward phytoplankton migration during a cold spell within the Late Cretaceous super-greenhouse. *Biogeosciences*, 13, 2859–2872. <https://doi.org/10.5194/bg-13-2859-2016>
- Voigt, S., Gale, A. S., & Flögel, S. (2004). Midlatitude shelf seas in the Cenomanian-Turonian greenhouse world: Temperature evolution and North Atlantic circulation. *Paleoceanography*, 19, PA4020. <https://doi.org/10.1029/2004PA001015>
- Witt, M. L., Mather, T. A., Pyle, D. M., Aiuppa, A., Bagnato, E., & Tsanev, V. I. (2008). Mercury and halogen emissions from Masaya and Telica volcanoes, Nicaragua. *Journal of Geophysical Research*, 113, B06203. <https://doi.org/10.1029/2007JB005401>
- Zheng, X., Jenkyns, H. C., Gale, A. S., Ward, D. J., & Henderson, G. M. (2013). Changing ocean circulation and hydrothermal inputs during Ocean Anoxic Event 2 (Cenomanian-Turonian): Evidence from Nd-isotopes in the European shelf sea. *Earth and Planetary Science Letters*, 375, 338–348. <https://doi.org/10.1016/j.epsl.2013.05.053>
- Zheng, X. Y., Jenkyns, H. C., Gale, A. S., Ward, D. J., & Henderson, G. M. (2016). A climatic control on reorganization of ocean circulation during the mid-Cenomanian event and Cenomanian-Turonian oceanic anoxic event (OAE 2): Nd isotope evidence. *Geology*, 44, 151–154. <https://doi.org/10.1130/G37354.1>

## Erratum

In the originally published version of this article, Figure 6 contained a minor formatting error. The figure has since been corrected, and this version may be considered the authoritative version of record.